

## Graphical Abstract

### **Image Inpainting based on Visual-Neural-Inspired Specific Object-of-Interest Imaging Technology**

Yonghao Wu, Chang Liu, Vladimir Filaretov, Dmitry Yukhimets

## Highlights

### **Image Inpainting based on Visual-Neural-Inspired Specific Object-of-Interest Imaging Technology**

Yonghao Wu, Chang Liu, Vladimir Filaretov, Dmitry Yukhimets

- Research highlight 1
- Research highlight 2

# Image Inpainting based on Visual-Neural-Inspired Specific Object-of-Interest Imaging Technology

Yonghao Wu, Chang Liu\*, Vladimir Filaretov, Dmitry Yukhimets

*School of Electronic Science and Engineering (School of Microelectronics), South China Normal University, Foshan, 528000, China*

*St. Petersburg School of Shipbuilding and Ocean Technology, Guangdong Ocean University, Zhanjiang 524088, China*

*Robotics Laboratory, Institute of Automation and Control Processes, Far Eastern Branch of the Russian Academy of Sciences, Vladivostok, 690041, Russia*

*Robotic Laboratory, Institute of Automation and Control Processes FEB RAS, Vladivostok, 690041, Russia*

---

## Abstract

Conventional image inpainting methods operate on whole images. Drawing on cortical processing principles this study addresses the bottlenecks of conventional holistic image inpainting methods—susceptibility to informational redundancy and low computational efficiency under occlusions and complex backgrounds, by proposing a novel framework: "Specific Object-of-Interest Imaging". This stage extracts and encodes object-level representations from complex scenes, generating semantic and structural priors that can be seamlessly integrated into any inpainting framework. On our Teapot object dataset, Elephant object dataset, Giraffe object dataset and Zebra object dataset experimental validation demonstrates—compared with the repair model without using this method, the repair model using this method has more advantages, across metrics including SSIM, PSNR, MAE, and LPIPS, while maintaining robustness in extreme scenarios (low illumination, high noise, multi-object occlusion, motion blur). Theoretical analysis integrated with cognitive neuroscience perspectives reveals profound correlations be-

---

\*Correspondence: liuchang@gdou.edu.cn

tween the "object precedence perception" mechanism and dynamic feature modulation in visual cortices (V1–V4). We demonstrate that incorporating Stage I significantly enhances object consistency and semantic coherence across various mainstream inpainting models. This work not only achieves efficient and precise target-centric imaging but also pioneers interdisciplinary pathways bridging brain-inspired computational frameworks with advanced image inpainting techniques.

*Keywords:* Image Inpainting, Specific Object-of-Interest Imaging, Visual Neural Mechanisms, Deep Neural Network

---

## 1. Introduction

Image Inpainting, a foundational and critically important task in computer vision and image processing, aims to restore missing or corrupted regions. Such impairments may arise from accidental occlusions during capture, sensor-induced noise, data loss in encoding/decoding or transmission, intentional object removal in post-processing, or physical deterioration in historical photographs. The capacity to restore image integrity, visual authenticity, and semantic plausibility renders this technology indispensable across diverse applications, including cultural heritage preservation, digital photography enhancement, medical image reconstruction, cinematic visual effects production, and the interpretation of occluded scenarios in autonomous driving systems. However, producing highly accurate and semantically coherent inpainting results remains a fundamental challenge.

Conventional inpainting methods primarily rely on intrinsic statistical properties and local structural information of images [1–8]. Canonical approaches include diffusion- and patch-based algorithms, whose core principle involves leveraging neighborhood information from intact regions to fill missing areas via propagation or copy-paste mechanisms. While adequate for small-scale, texturally regular regions, these methods exhibit significant limitations when confronted with extensive missing areas, complex structural boundaries, or semantically rich regions. They often generate artifacts such as blurred textures, fractured structural continuity, and semantically inconsistent content that undermines global image context. These limitations significantly constrain their effectiveness in real-world, high-fidelity imaging applications.

The rapid development of deep learning—particularly Convolutional Neural Networks (CNNs), Generative Adversarial Networks (GANs), and emerging

Transformer- and Diffusion-based models—has driven breakthroughs in complex pattern learning and high-fidelity image synthesis, thereby catalyzing a paradigm shift in image inpainting [9–15]. These data-driven approaches capture rich image priors and deep semantic representations from large-scale datasets, thereby enabling models to predict missing content with improved accuracy. These models reconstruct intricate textural details while maintaining plausibility. For example, restored objects exhibit geometrically consistent structures, physically coherent illumination, and contextually appropriate depth relationships. State-of-the-art models can generate diverse yet equally plausible results, demonstrating performance that substantially surpasses conventional methods.

Despite these advances and their widespread deployment, researchers still face persistent and critical challenges. A pivotal yet often overlooked issue is the inefficiency and inaccuracy stemming from informational redundancy. In many real-world applications, inpainting is fundamentally object-centric rather than indiscriminately processing the entire frame. Under such conditions, prevailing whole-image inpainting models — encompassing nearly all contemporary deep learning methods — incur substantial computational overhead by processing redundant background information. For instance, autonomous vehicles equipped with 8K cameras can generate up to 1.5 TB/s of data, with nearly 90% consisting of redundant background or irrelevant content; military reconnaissance satellites transmit massive raw imagery, with less than 0.1% containing actionable intelligence; and in medical X-ray imaging and industrial non-destructive testing, conventional area-array detectors achieve less than 0.13% efficiency in extracting useful information. Whole-image models consume substantial computational resources analyzing redundant background information, leading to severe resource wastage and reduced accuracy in target-object reconstruction due to background interference, calling for a paradigm shift from holistic processing to targeted, object-focused inference.

In confronting these challenges, biological vision systems offer an elegant and efficient solution. A core component of biological vision is the attention mechanism, which prioritizes task-relevant targets while suppressing redundant background information. This enables efficient, accurate, and energy-optimized information processing for target recognition and imaging in cluttered or dynamic scenes. This “object-first perception” strategy offers a promising solution for addressing low information density and background noise in inpainting: an inpainting pipeline could first localize and model

target-object structures while excluding irrelevant background as interference. Such an approach would enhance imaging focus, computational efficiency, and output quality.

Building on this analysis of the current state of inpainting, its technical bottlenecks, and biological inspiration, we propose a novel front-end paradigm: Image Inpainting via Visual-Neural-Inspired Specific Object-of-Interest Imaging technology(SIOI). Inspired by biological “object-first perception”, we propose a paradigm shift: Specific Object-of-Interest Imaging (SIOI). Unlike traditional methods, SIOI decouples the ‘what’ and ‘where’ of the object from the ‘how’ of its inpainting. It acts as a generic front-end that extracts a clean object representation, suppressing background noise, and can be plugged into any existing inpainting model. Our framework decomposes the imaging process into two distinct stages. Stage 1 focuses exclusively on extracting and modeling the structural information of target objects. This stage constitutes a dedicated information-extraction process designed to maximize target-relevant features while minimizing or eliminating background interference. Stage 2 performs coarse structural restoration guided by refined priors to support detail synthesis, refines the restoration, ensuring visual coherence and semantic consistency in the final output. The key innovation lies in Stage I; Stage II is deliberately kept simple in our experiments to prove the concept. By frontloading SIOI, the pipeline significantly reduces background distractions and concentrates structural modeling on critical target regions. This substantially reduces the data volume for processing, thereby improving computational efficiency while enhancing structural continuity and semantic accuracy. As shown in Tab. 1, unlike other image-restoration methods, this bio-inspired approach aligns with the hierarchical modeling of the visual cortex in neural networks, ensuring that computational efficiency parallels human attentional selection.

Our principal contributions are:

1. We introduce Specific Object-of-Interest Imaging (SIOI), a novel front-end paradigm for object-centric image processing. SIOI explicitly decouples target-object extraction from texture synthesis, providing a generic mechanism to reduce background interference and generate powerful structural priors for any subsequent task.
2. We conduct a preliminary exploration of correlations between human vision and deep networks, integrating neuroscientific and psychological insights on hierarchical visual cortex processing to establish theoretical

foundations.

3. We demonstrate that SIOI is an effective, plug-and-play front-end module. Through extensive experiments, we show that integrating SIOI consistently enhances the performance of various mainstream inpainting models across multiple metrics and datasets, while significantly improving robustness in extreme scenarios.

Table 1: Theoretical Framework Comparison

Model	Theoretical Framework	Core Mechanism	Processing Unit	Biological Plausibility
Traditional	Digital image processing and classical machine learning techniques	Handcrafted features and algorithms	Entire image	Not considered
Deep-Learning	Data-driven approaches enabled by deep neural networks	Learned feature representations	Entire image	Not considered
Ours	<b>Bio-inspired two-stage framework</b>	<b>Object perception → Object inpainting</b>	Specific Object-of-Interest	<b>V1-V4 hierarchical simulation</b>

## 2. Related Works

Image inpainting is a long-studied and widely applied problem whose methods have undergone substantial paradigm shifts. From early mathematical models to modern deep generative architectures. While these approaches differ in implementation, they overwhelmingly share a whole-image processing paradigm.

### 2.1. Traditional Mathematical Algorithms: Digital Image Processing and Machine Learning

This period emphasized leveraging low-level statistical properties, local geometric structures, and hand-crafted mathematical models. Representative approaches include: 1) PDE- and diffusion-based models [1, 16, 17], which use isophote directions or engineered diffusion tensors to propagate color and gradient information from intact regions into missing areas while preserving

edge coherence; and 2) patch-based methods [18–20], which exploit non-local self-similarity by searching for patches in intact regions that best match neighborhoods around missing regions and iteratively copying them to fill holes. Traditional mathematical approaches [21–23] reconstruct missing areas by propagating local structures or copying similar patches. They perform reasonably on small, regular textures but break down under large occlusions or semantically rich regions, since they lack object-level understanding.

## 2.2. Data-Driven Neural Network Approaches

Deep-learning approaches substantially improve structural coherence and realism by learning high-level priors. Predominant paradigms include: (1) CNN encoder–decoder architectures [4, 24–27], which exploit multi-level encoder features to progressively generate missing content in decoders, attention mechanisms and gated convolutions further improve focus on relevant regions; (2) GAN-based methods [28–34], which employ adversarial training between generators and discriminators to produce highly realistic outputs and excel at fine texture synthesis and alignment with natural image distributions; (3) Transformer-based approaches [4, 35–40], which leverage self- and cross-attention to model long-range dependencies between patches and thereby capture global semantics and structural consistency, improving performance on complex scenes and large corruptions; and (4) diffusion models [41–43], which cast generation as a progressive denoising process that iteratively recovers image details from noise, offering fine-grained detail control, diverse outputs, and high fidelity.

Yet, most still operate on the entire image, wasting computation on irrelevant background and suffering from interference when target and background overlap. Crucially, they rarely encode explicit object guidance, limiting their ability to ensure object consistency in inpainting. Whole-image models thus suffer from several issues in object-centric tasks: 1) information redundancy and computational inefficiency — processing the entire image wastes computation on irrelevant background content, exacerbating the low effective information density typical in domains such as autonomous driving and satellite imaging; 2) background interference — complex or misleading backgrounds can corrupt the reconstruction of target object structure and semantics, especially when target and background share similar textures or colors; and 3) lack of target-specific guidance and focus — current methods rarely model explicitly which object should be targeted and therefore struggle to separate target signals from background noise during inpainting. Although

some methods adopt user sketches or bounding boxes as guidance, these require extra interaction and still struggle to achieve precise target separation in complex scenes.

Thus, a biologically inspired, target-focused imaging paradigm — one that actively suppresses irrelevant background information — is imperative for object-centric tasks. Our proposed method, *Inpainting via Specific Object-of-Interest Imaging*, directly addresses this gap. It introduces a front-loaded Specific Object-of-Interest Imaging module that algorithmically maximizes target-relevant information while suppressing background interference. This yields highly refined, target-centric signals for subsequent inpainting stages and thereby mitigates information redundancy and background interference.

### 2.3. Insights from Human Visual Mechanisms for Image imaging

Psychologists and neuroscientists have reported direct correlations between deep neural networks (DNNs) and hierarchical processing in the visual cortex [44, 45]. Human vision follows a hierarchical pathway: retina → lateral geniculate nucleus (LGN) → V1 (edge extraction) → V4 → IT (semantic processing) [46, 47]. This observation motivates multi-stage imaging networks [48, 49], in which early convolutional layers focus on local structure repair (analogous to V1 edge detection), while deeper layers integrate object identity and scene context (analogous to IT semantic processing); skip connections can be viewed as a crude analogue of cortical feedback. Predictive-coding theory [50, 51] proposes that the brain leverages prior knowledge (e.g., Gestalt principles) to generate predictions and correct sensory errors. This idea parallels the generator–discriminator framework in deep inpainting [4, 24]: generators predict missing content by learning data distributions, while discriminators enforce semantic plausibility via adversarial training [52]. At the level of attentional regulation, bottom-up attention captures salient features (e.g., high-frequency details) via thalamic structures such as the pulvinar [53, 54]; this motivates algorithmic mechanisms such as saliency-map-weighted losses that emphasize abrupt edge regions [55]. Conversely, top-down attention involves prefrontal-cortex (PFC) modulation of visual responses according to task goals [54]. This inspires task-oriented strategies in models: for example, conditional vectors can steer generation to enhance discriminative feature repair (e.g., facial keypoint reconstruction) and to improve global structural consistency for scene reconstruction. Examples of biologically inspired techniques include contour interpolation via edge-consistency losses [56], motivated by V1/V2 responses to illusory contours

[57–59]. Semantic guidance has been realized by mapping IT-like object activations. For instance, CLIP-guided diffusion has been used to align textual concepts with image generation [42]. Memory-augmented imaging methods simulate hippocampal–cortical episodic recall by retrieving reference segments from external memory banks [60]. Consequently, advancing image inpainting benefits from drawing principled inspiration from human visual mechanisms to identify promising directions for improvement. This ‘object-first’ perception allows efficient suppression of background noise and allocation of resources to relevant targets. Such mechanisms directly motivate our proposed Specific Object-of-Interest Imaging, which introduces an analogous front-end object-first module into the inpainting pipeline.”

In summary, while existing methods have advanced in realism and fidelity, they all share a whole-image bias that is ill-suited for object-centric tasks. Inspired by biological vision, we propose a new front-end paradigm—Specific Object-of-Interest Imaging—to fill this critical gap.

### 3. Proposed Methodology

This section delineates our proposed framework for Image Inpainting. Our approach introduces a novel paradigm for this task. On a conceptual level, it shares a similar goal—focusing on a specific object region—with other imaging techniques, such as [61–65], but the underlying methodology is uniquely our own work. The processing pipeline is illustrated in Fig. 1.

#### 3.1. Specific Object-of-Interest Imaging

Specific Object-of-Interest Imaging is also known as Attention-Targeted Imaging. Desimone and Duncan’s competitive-bias model [66] posits that multiple objects compete for activation resources in the visual cortex. Attention serves as a bias signal that preferentially amplifies target objects and suppresses background information. This provides a neuroscientific foundation for implementing background suppression and object-enhancement saliency selection in computational networks. O’Craven et al. [67] demonstrated with fMRI that objects act as fundamental attentional units, exhibiting holistic enhancement even when component features are spatially segregated. Other studies [68, 69] further showed that object boundaries automatically attract attention, recruiting V1–V4 regions and intensifying internal feature encoding. Perry et al. [70] reported that foveal cortical magnification increases encoding density, and that task-dependent plasticity enables high-resolution perception

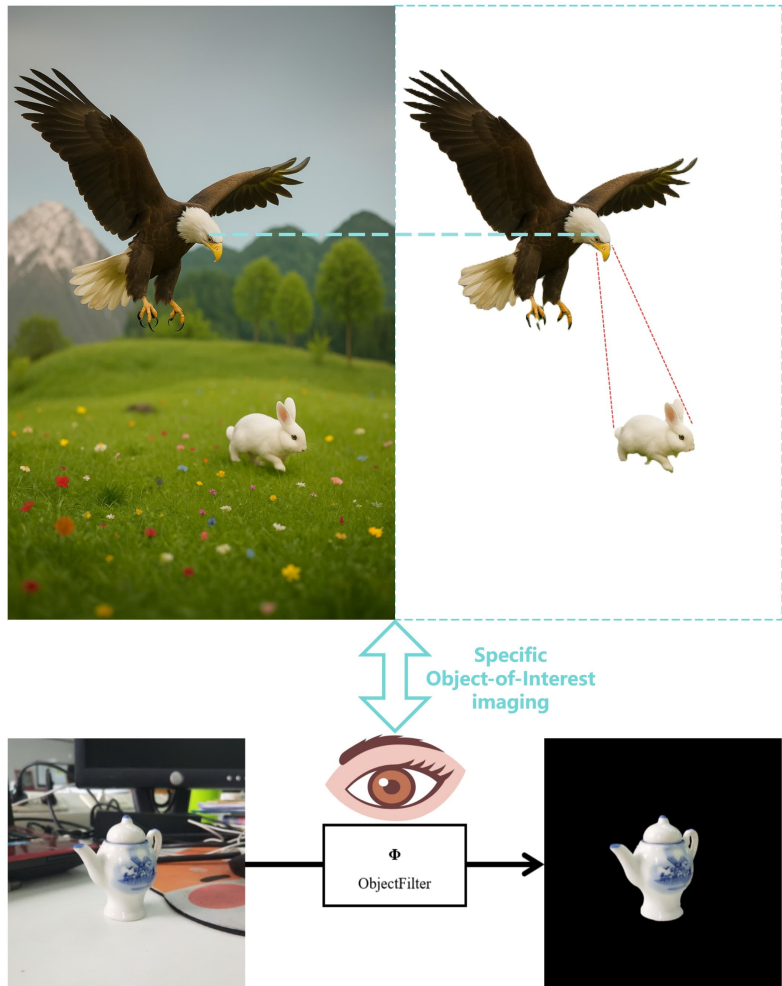


Figure 1: Specific Object-of-Interest Imaging technology.

of behaviorally relevant regions. Carrasco and Barbot [71, 72] systematically characterized attention’s dual regulation of spatial resolution: exogenous attention enhances frequency sensitivity at fixation loci, whereas endogenous attention reallocates resolution according to task demands. Barbot and Carrasco further showed that attentional guidance amplifies high-frequency recognition, providing a basis for region-adaptive reconstruction. Ekman et al. [73] demonstrated that attentional signals propagate along object boundaries in V1, inducing internal feature enhancement — a phenomenon translatable to frequency-domain focusing mechanisms in networks (e.g., concentrating computational resources using object masks). Collectively, these findings reveal an object-based prioritization mechanism: the visual system preferentially allocates resources to enhance detailed representation of target objects. These observations directly inspired our object-detection-guided saliency-enhancement branch, which applies high-frequency component weighting to target regions. We propose an approach that integrates saliency modeling with biologically inspired, object-guided image imaging to construct a cognitively plausible, interpretable, and task-relevant image inpainting system (see Fig. 2).

Neuroanatomically, visual processing follows a hierarchical architecture: local feature detection (retina)  $\rightarrow$  spatial integration (LGN)  $\rightarrow$  orientation selectivity (V1)  $\rightarrow$  holistic object representation (IT cortex). This multi-stage processing implies that a natural-scene image  $k$  can be viewed as a superposition of multiple latent target objects, with attentional modulation in V4 amplifying target-specific features while suppressing background information. Grounded in neuronal population-coding theory and Hebbian plasticity, we formalize this composition as a linear superposition model:

$$k = \sum_{i=1}^M \{k_i\} \quad (1)$$

where  $k \in \mathbb{R}^{H \times W \times C}$  denote the scene tensor,  $k_i \in \mathbb{R}^{h_i \times w_i \times C}$  the  $i$ -th target object, and  $M \in \mathbb{Z}^+$  the total number of objects. Each  $k_i$  corresponds to a semantically complete entity in the scene (e.g., pedestrians or vehicles). Amodal content completion emphasizes restoring full object structures in occluded regions. The core objective is anatomically precise object separation: accurately extracting specific targets  $k_i$  ( $i \in \{1, \dots, M\}$ ) from complex backgrounds. This parallels the “cocktail-party” effect in human perception when attending to a target in cluttered scenes.

To overcome the representational fragility of traditional methods in noisy

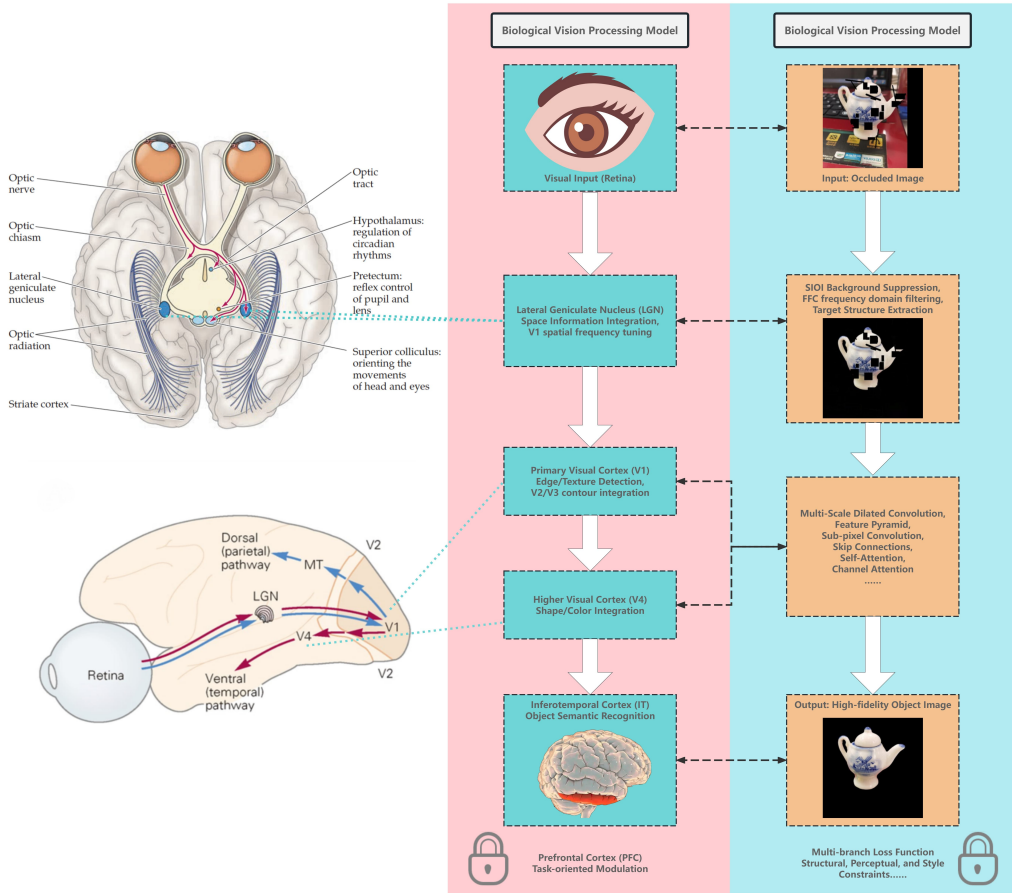


Figure 2: Image inpainting framework based on the visual neural Specific Object-of-Interest Imaging.

environments, we propose a biologically inspired dynamic feature-modulation paradigm. Its mathematical core is a target-sensitive measurement matrix  $\Gamma$ . Via a differentiable learning mechanism,  $\Gamma$  induces a cross-scale feature set  $\{\xi_j\}_{j=1}^N$ , reflecting the hierarchical abstraction from V1 simple cells (edge/texture responses) to IT complex cells (holistic shape responses). Below we make these notions precise.

For a target index  $\mu \in \{1, \dots, M\}$ , we write

$$\Gamma k_\mu = \sum_{j=1}^N \omega_{j,\mu} \xi_j, \quad (2)$$

where  $\Gamma \in \mathbb{R}^{N \times D}$  denotes the measurement matrix,  $\xi_j \in \mathbb{R}^D$  the feature-basis vectors, and  $\omega_{j,\mu} \in \mathbb{R}$  the feature weights associated with target  $\mu$ . When optimization drives the object- and target-specific weights  $\omega_{j,\mu}$  to concentrate on the feature patterns of a particular  $\mu$ , the system exhibits a selective-gain effect: scene measurements become dominated by target-related information flow. These dynamics are expressed as

$$\Gamma k = \begin{bmatrix} \sum_{m=1}^M \eta_{1,m} \xi_1 \\ \vdots \\ \sum_{m=1}^M \eta_{N,m} \xi_N \end{bmatrix} \approx \hat{k}_\mu, \quad (3)$$

where  $\eta_{j,m}$  denotes the contribution of object  $m$  to feature channel  $j$ . Measurements concentrate on the specific target when  $\eta_{j,m} \rightarrow \delta_{m\mu}$  for each feature channel  $j$ , i.e., when the contributions from non-target objects vanish.

Functionally, this formulation mirrors the hierarchical transformation from V1 simple cells (edge/texture responses) to IT complex cells (holistic shape responses), with  $\Gamma$  playing the role of attentional gain control in V4. V1 encodes local orientations, while V4 integrates global contours under top-down modulation, consistent with our FFC-based frequency-domain focusing. From a functional-analysis perspective, this process can be interpreted as a target-guided modulation on an appropriate Riemannian manifold:

$$\Gamma k = \sum_{m=1}^M \Gamma \omega_m \otimes k_m \approx \hat{k}'_0 \quad (4)$$

where  $\otimes$  denotes the diffeomorphism operator in the feature space. Establishing a rigorous mathematical model is essential for precise object separation.

Consider an input scene containing  $N$  latent targets. Sparse representation of individual objects. Each object  $k_i$  ( $i = 0, 1, \dots, N - 1$ ) can be represented sparsely in a high-dimensional dictionary basis  $\Psi$ :

$$k_i = \sum_{j=1}^M \psi_{ij} x_{ij} \quad (5)$$

where  $\psi_{ij}$  denotes the adaptive sparse basis and  $x_{ij}$  the sparse coefficients. Panoramic scene decomposition indicates that the holistic scene can be expressed as a linear combination of objects:

$$k = \sum_{i=0}^{N-1} k_i = \sum_{i=0}^{N-1} \sum_{j=1}^M \psi_{ij} x_{ij} \quad (6)$$

subject to the following constraints:  $\|\mathbf{x}_i\|_0 \ll M$  (Sparsity),  $\psi_{ij} \in \mathbb{R}^D$  (Dictionary Basis),  $x_{ij} \in \mathbb{R}$  (Sparse Coefficient). This representation satisfies the principles of compressed sensing, thereby ensuring object separability in the feature space. This theoretical model is implemented through a bio-inspired neural architecture. The Feedforward Feature Selection Network simulates the ventral (“what”) visual pathway by performing target-sensitive filtering on masked defective inputs  $M_h$ . The Target Reconstruction Network mimics the spatial integration function of the parietal cortex and is dedicated to target reconstruction. The training process is formulated as a physically constrained optimization problem:

$$\{\xi, \theta\} = \arg \min \frac{1}{H} \sum_{h=1}^H \mathcal{C}(N_h, \tilde{N}_h) \quad (7)$$

where  $\mathcal{C}(\cdot)$  denotes the loss function. Upon convergence, the FECNet weights  $\xi$  encode target knowledge into a feature filter  $\phi$ . Applying  $\phi$  to the panoramic scene yields:

$$\phi k = \phi \left( \sum_{i=0}^{N-1} \sum_{j=1}^M \psi_{ij} x_{ij} \right) = \sum_{j=1}^M \psi_{0j} x_{0j} = \hat{k}_0 \quad (8)$$

Since  $\phi$  is a linear operator, it satisfies the following projection property:

$$\phi(x_{ij}) = \begin{cases} x_{0j}, & \text{if } i = 0 \\ 0, & \text{if } i \neq 0 \end{cases} \quad (9)$$

Assume the dictionary  $\Psi$  satisfies the Restricted Isometry Property (RIP), i.e.  $\text{RIP}(\Psi) \leq \delta_{2s}$  (separability condition). The underlying mechanism is that the filter  $\phi$  implements an (approximate) orthogonal complement in feature space,  $\phi = I - P_{\text{bg}}$ , thereby suppressing non-target components (i.e., those with  $i \neq 0$ ).

A closed-form estimator for  $\phi$  can be obtained by minimizing a least-squares criterion and expressed via the Moore–Penrose pseudoinverse. Defining  $k^{(h)}$  as the vectorized scene for sample  $h$  and  $\hat{k}_0^{(h)}$  as its corresponding target component, we may write

$$\begin{aligned} \phi &= \arg \min_{\phi'} \sum_h \left\| \hat{k}_0^{(h)} - \phi' \left( \sum_{i=0}^{N-1} k_i^{(h)} \right) \right\|_F^2 \\ \Rightarrow \quad \phi &= \left( \sum_h \hat{k}_0^{(h)} k^{(h)T} \right) \left( \sum_h k^{(h)} k^{(h)T} \right)^{\dagger} \end{aligned} \quad (10)$$

where  $\dagger$  denotes the Moore–Penrose pseudoinverse, and  $k^{(h)} \in \mathbb{R}^{D \times 1}$  is the vectorized scene representation for sample  $h$ . We further constrain  $\phi = \mathbf{I} - \mathbf{P}_{\text{bg}}$  as an (approximate) orthogonal projection onto the target subspace.

Equivalently,  $\phi$  may be viewed as the best approximation to the ideal projection  $I - P_{\text{bg}}$  in a suitable Hilbert space  $\mathcal{H}$ :

$$\phi^* = \arg \min_{\phi \in \mathcal{H}} \left\| \phi - (I - P_{\text{bg}}) \right\|_F. \quad (11)$$

Here  $\mathcal{H}$  is a Hilbert space with inner product  $\langle \cdot, \cdot \rangle$  and induced norm  $\|\cdot\|$ ;  $\|\cdot\|_F$  denotes the Frobenius norm for matrices,  $\|A\|_F = \sqrt{\sum_i \sum_j |a_{ij}|^2}$ .

Let  $\mathbf{q}_{xy}$  and  $\mathbf{k}_{ij}$  denote learned query and key feature vectors at spatial locations  $(x, y)$  and  $(i, j)$ , respectively, and let  $d$  be the feature dimensionality used for softmax scaling. Under bio-inspired attentional modulation we compute attention weights by

$$\alpha_{xy} = \frac{\exp(\langle \mathbf{q}_{xy}, \mathbf{k}_{ij} \rangle / \sqrt{d})}{\sum_{i,j} \exp(\langle \mathbf{q}_{xy}, \mathbf{k}_{ij} \rangle / \sqrt{d})}, \quad (12)$$

where the denominator normalizes over all spatial locations  $(i, j)$ . When  $\mathbf{q}_{xy}$  and  $\mathbf{k}_{ij}$  are highly similar, the corresponding attention weight  $\alpha_{xy}$  approaches one, consistent with Feature Integration Theory: biased competition in V4 enhances target features via attentional gain.

Require that the Kullback–Leibler divergence between the target and background distributions satisfies

$$D_{\text{KL}}(P_{\text{target}} \| P_{\text{background}}) > \sum_{i=2}^M D_{\text{KL}}(P_{\text{target}} \| P_{\text{object}_i}), \quad (13)$$

where  $D_{\text{KL}}(P \| Q) = \sum_i P_i \log \frac{P_i}{Q_i}$  denotes the Kullback–Leibler divergence.

By large-deviation principles, when the distributional discrepancy between the target and background dominates inter-object interference, empirical distributions concentrate on distributions minimizing relative entropy; consequently, the estimator tends to concentrate on the target distribution, which implies reduction of the estimated target entropy under suitable conditions. Hence, under these assumptions there exists a unique solution  $\hat{k}_0$  such that

$$\lim_{t \rightarrow \infty} H(\hat{k}_0^{(t)}) = H_{\text{target}}, \quad (14)$$

where  $H(X) = -\sum_{x \in \mathcal{X}} p(x) \log p(x)$  denotes the Shannon entropy.

Under Assumptions A1–A3 (sparsity of object representations, the RIP on dictionary  $\Psi$ , and bounded measurement noise), there exists a linear operator  $\phi$  (learnable by FECNet) that approximates the ideal target projector  $I - P_{\text{bg}}$ . By compressed-sensing theory, if  $\text{RIP}(\Psi) \leq \delta_{2s}$  then the learned projector  $\phi$  (approximating  $I - P_{\text{bg}}$ ) admits the error bound

$$\|\phi k - \hat{k}_0\|_2 \leq C_1 \sigma_s(k) + C_2 \epsilon, \quad (15)$$

where  $C_1$  and  $C_2$  depend on the RIP constants and the dictionary condition number;  $\sigma_s(k)$  denotes the error of the best  $s$ -term approximation of  $k$ ; and  $\epsilon$  denotes an upper bound on the measurement noise.

Together, these results provide a rigorous foundation for the proposed object-centric imaging approach. By casting target separation as a formal projection problem under sparsity constraints and employing information-theoretic concentration arguments to characterize convergence, we show that under the stated assumptions the Specific Object-of-Interest Imaging system provably isolates the target and converges to an optimal reconstruction that up to the approximation and noise terms given above.

### 3.2. Image Inpainting System

To enhance structural coherence and reconstruction accuracy for occluded images, we propose a two-stage framework grounded in specific-object-of-

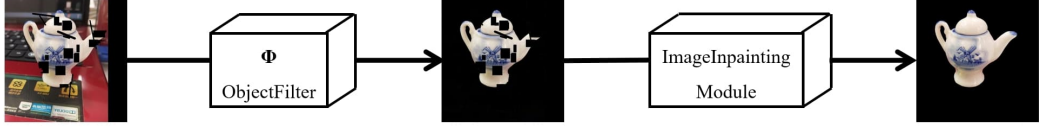


Figure 3: Processing flow of the proposed image-inpainting system.

interest imaging principles (Fig. 3). Departing from traditional pixel-level completion in RGB space, our architecture adopts an object-first perception inspired by biological vision, decomposing the task into structure-prioritized progressive refinements. Emphasizing semantically coherent reconstruction, we decompose the imaging pipeline into two stages: (1) object perception  $\rightarrow$  (2) object inpainting. The core innovation is SIOI, which compels the model to focus on the target object while suppressing irrelevant background interference. This reduces computational overhead by concentrating structural modeling on critical regions (see Fig. 4).

**Stage I: Specific Object-of-Interest Imaging** Biological vision begins with retinal photoreceptors converting incoming light into neural signals. Subsequent processing in the lateral geniculate nucleus (LGN) integrates spatial information and suppresses high-frequency noise via center-surround antagonism. Feature extraction proceeds in primary visual cortex (V1), where simple cells respond to oriented edges and spatial-frequency textures [46]. Object prioritization amplifies target representations through bottom-up attentional biasing [66], suppressing background interference—functionally analogous to selective attention in the "cocktail-party" effect.

Our SIOI module computationally embodies this hierarchy. We process corrupted inputs with modified U-Net encoders to extract multi-scale features, mimicking V1 orientation selectivity. Embedding Fast Fourier Convolution (FFC) modules in multiple encoding and decoding processes captures long-range dependencies through spectral transformation, simulating attentional modulation in V4 that amplifies target signals. The spectral processing can be written as

$$\mathcal{F}_{\text{freq}} = \text{Conv}_{\text{freq}}(\text{FFT2}(\mathcal{F})), \quad \mathcal{F}' = \text{IFFT2}(\mathcal{F}_{\text{freq}}), \quad (16)$$

where FFT2 and IFFT2 denote the 2-D Fourier transform and its inverse, respectively, and  $\text{Conv}_{\text{freq}}$  is a learnable convolutional operator applied in the frequency domain. (Fig. 5)

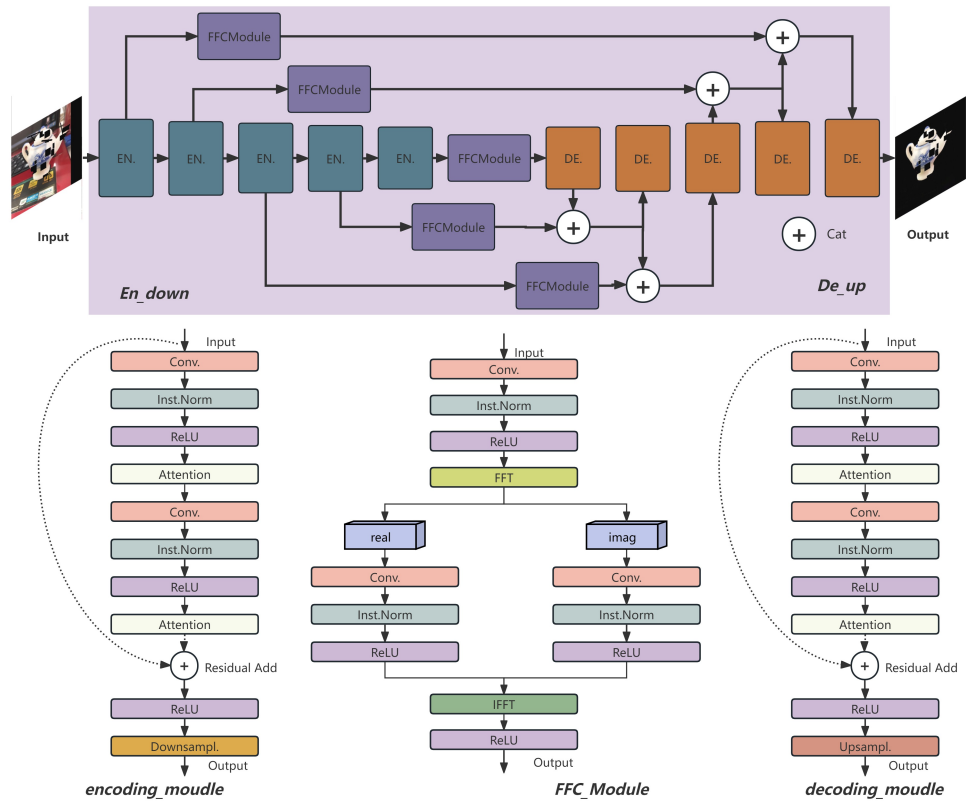


Figure 4: Architecture of the proposed Specific Object-of-Interest Imaging.

The output of the SIOI module is a preliminary, yet structurally coherent, object map contain local defects. As shown in Fig. 4. Biologically, this parallels V1 edge detection and V4-mediated object-based attention, in which attentional gain enhances target representations while suppressing background activity [74]. Our FFC modules enhance target-relevant spectral components while attenuating background spectra. Functionally, FFC operations correspond to V1-like orientation detection, whereas the learned attention weights emulate pulvinar–thalamic modulation of cortical processing. Consequently, Stage I produces structurally coherent object maps despite occlusions, providing essential priors for subsequent texture synthesis and refinement. This spectral processing overcomes the limitations of standard convolutions for modeling long-range dependencies and significantly improves structural consistency.

Together, these mechanisms reduce information redundancy. The SIOI module serves as a generic, front-end "visual processor" that transforms a complex, occluded scene into a purified, object-centric representation. It provides a powerful intermediate representation that is the cornerstone of our framework, explicitly containing the structural and semantic priors necessary for high-fidelity inpainting.

### Stage II: Object Inpainting (Coarse inpainting + Fine inpainting)

To validate the efficacy of the SIOI module independently of advanced inpainting architectures, we deliberately employ a straightforward inpainting network in Stage II. Unlike conventional image inpainting methods, our model eliminates the need for additional manually annotated corruption masks and is capable of automatically identifying and inpainting the corrupted regions of the target. It is critical to emphasize that the innovation of this work is not this network itself, but rather the SIOI module. The purpose of Stage II is solely to demonstrate that the priors generated by SIOI are so potent that they enable even a simple network to achieve high-quality reconstruction. This stage is loosely analogous to the role of higher visual areas in integrating semantic information for detailed perception. Our Structural Recovery Module (SRM) takes the SIOI output and performs contour interpolation and shape completion using multi-scale dilated convolutions and feature-pyramid fusion:

$$\mathcal{F}_{MSDC} = \text{Concat} \left( \bigcup_{r \in \{1,2,4,6\}} \text{Conv}_r(x) \right) \quad (17)$$

An FPN-like fusion integrates encoder–decoder hierarchical features, and

subpixel-convolution upsampling is used to suppress checkerboard artifacts. The output is a complete structural feature tensor  $\mathcal{F}_{\text{SRM}} \in \mathbb{R}^{64 \times H \times W}$ .

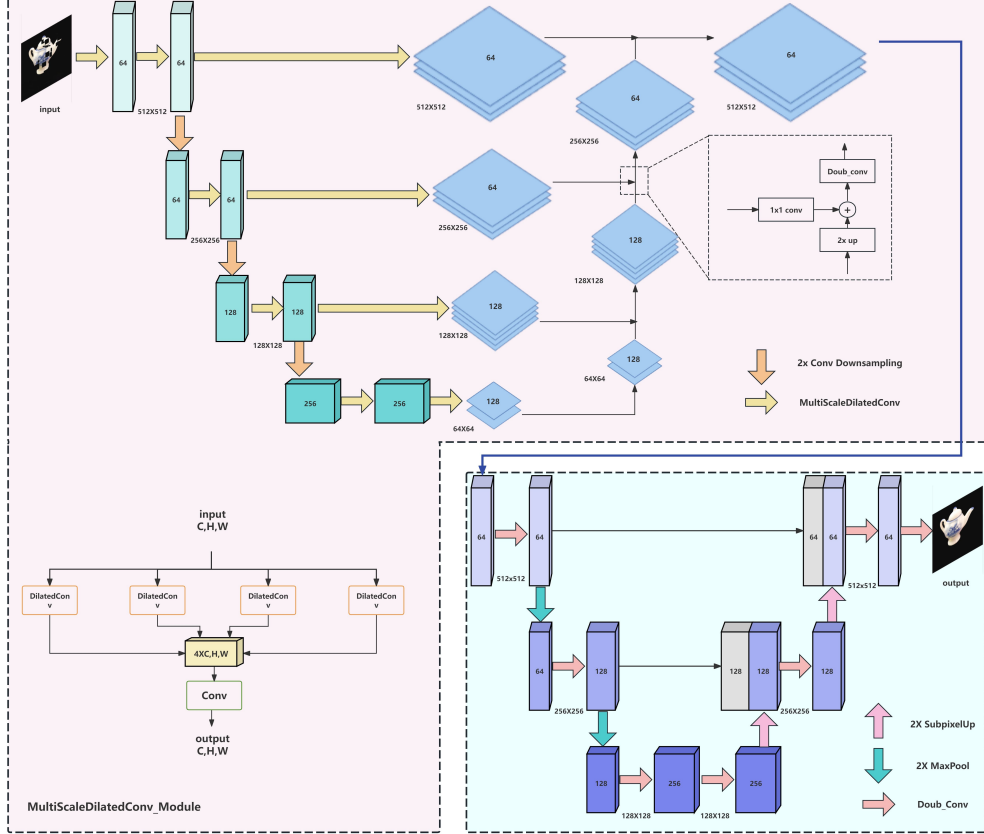


Figure 5: Architecture of the Simple Object Inpainting.

Functionally, both biological and computational systems achieve structural coherence: biological vision generates shape priors via predictive-coding [50], while the SRM fuses multi-scale context through MSDC and feature-pyramid fusion. This design helps to avoid texture blurring and semantic mismatches. Technically, MSDC operations correspond to V2–V3 contour integration, while feature-pyramid fusion approximates cortical feedback modulation. SRM enhances structural integrity in partially occluded object maps from Stage I, enabling a coarse-to-fine imaging strategy.

$$\mathcal{F}_{\text{SRM}} = \mathcal{R}(I_{\text{coarse}}), \quad \mathcal{F}_{\text{SRM}} \in \mathbb{R}^{64 \times H \times W}, \quad (18)$$

where  $\mathcal{R}(\cdot)$  denotes SRM processing and  $I_{\text{coarse}}$  denotes the coarsely restored map. Subsequently, the Global Detail Recovery Module (GDRM) utilizes a symmetric encoder-decoder with skip connections to synthesize fine-grained textures onto the recovered structure, guided by the robust priors from Stage I. Our computational counterpart, the Global Detail Recovery Module, implements a symmetric encoder-decoder architecture that consumes the 64-channel structural features  $\mathcal{F}_{\text{SRM}} \in \mathbb{R}^{64 \times H \times W}$  produced by the SRM. This simple design choice underscores our core claim: The SIOI module is a versatile, plug-and-play component that can elevate the performance of any existing inpainting pipeline by providing superior object-specific guidance.

### 3.3. Loss function

To achieve high-fidelity reconstruction of defective object images, we design a multi-branch fused loss that jointly promotes structural coherence, fine-detail reconstruction, and global visual-style consistency. The composite loss comprises three components: a weighted reconstruction loss [48, 75], a perceptual loss [76], and a style loss [77]. Integrated with principled weighting and multi-stage optimization strategies, the loss ensures that synthesized images exhibit improved semantic structure and textural fidelity.

**Weighted Reconstruction Loss.** We introduce a spatially weighted reconstruction loss based on target maps. An explicit weight map  $w(x, y)$  differentially weights per-pixel reconstruction errors in the  $L_1/L_2$  terms:

$$\mathcal{L}_{\text{weighted}} = \frac{1}{N} \sum_{x,y} (\alpha w(x, y) + 1) \|\hat{I}(x, y) - I_{\text{gt}}(x, y)\|_2^2 \quad (19)$$

Equivalently, at pixel-level the reconstruction loss can be written as

$$\mathcal{L}_{\text{recon}} = \sum_i w_i \|I_i^{\text{pred}} - I_i^{\text{gt}}\|_2^2, \quad (20)$$

where  $\hat{I}(x, y)$  denotes the predicted intensity at pixel  $(x, y)$ ,  $I_{\text{gt}}(x, y)$  the corresponding ground truth,  $I_i^{\text{pred}}$  and  $I_i^{\text{gt}}$  the RGB vectors at pixel  $i$ ,  $w_i$  the pixel-level weight, and  $\alpha$  a scalar weighting factor (empirically set to 4). Higher weights are assigned to semantic target regions and lower weights to background regions; this directs the network to prioritize detail reconstruction in structurally critical areas and effectively mitigates edge blurring and structural discontinuities. This mechanism intensifies supervision in target regions while reducing gradient interference from irrelevant areas.

**Perceptual Loss.** To compensate for pixel-level losses’ inability to capture high-level semantics, we incorporate a perceptual loss computed from feature activations of a pretrained VGG-16 network:

$$\mathcal{L}_{\text{perc}} = \sum_{l \in \mathcal{L}} \frac{1}{C_l H_l W_l} \|\phi_l(I^{\text{pred}}) - \phi_l(I^{\text{gt}})\|_2^2, \quad (21)$$

where  $\phi_l(\cdot)$  denotes the feature maps extracted from the  $l$ -th VGG-16 layer, and  $C_l, H_l, W_l$  denote the channel count, height, and width of  $\phi_l$ , respectively. By comparing representations across selected VGG-16 layers, the perceptual loss captures high-level semantics (e.g., object shapes and textures) and enhances semantic coherence in generated objects.

**Style Loss.** The style loss quantifies texture distribution and stylistic characteristics using Gram matrices as in style-transfer methods [77]. For feature maps  $\phi_l(x)$  at layer  $l$  of VGG-16, the Gram matrix is

$$G_l(x) = \phi_l(x) \phi_l(x)^\top, \quad (22)$$

and the style loss is

$$\mathcal{L}_{\text{style}} = \sum_{l \in \mathcal{L}} \|G_l(I^{\text{pred}}) - G_l(I^{\text{gt}})\|_F^2, \quad (23)$$

where  $\mathcal{L}$  denotes the set of selected layers and  $\|\cdot\|_F$  the Frobenius norm. This statistical matching captures local texture statistics and global stylistic discrepancies, improving the naturalness of restored images and reducing pattern repetition and artifacts.

**Composite Loss.** The integrated loss combines the above terms. The weighted reconstruction term enhances edge clarity and structural continuity in semantic regions; the perceptual term reinforces high-level semantic consistency aligned with human perception; and the style term mitigates texture artifacts across diverse objects and scenes:

$$\mathcal{L}_{\text{total}} = \lambda_1 \mathcal{L}_{\text{recon}} + \lambda_2 \mathcal{L}_{\text{perc}} + \lambda_3 \mathcal{L}_{\text{style}} \quad (\lambda_1 = 1.0, \lambda_2 = 0.1, \lambda_3 = 250) \quad (24)$$

These weights are empirically chosen to balance the differing numerical scales and competing objectives of the loss components during training.

## 4. Experiment

### 4.1. Dataset

Four distinct datasets were employed. A custom object-centric teapot dataset (2,000 training, and 200 test samples) constructed in our laboratory featuring  $512 \times 512$  scene images of multi-view teapot objects against complex backgrounds with artificial items and indoor environments, each paired with corresponding  $512 \times 512$  ground-truth masks that underwent multi-stage manual calibration to preserve geometric structures and textural details; alongside three COCO2017-derived subsets—“elephant” (2,143 training images, 89 validation as test), “giraffe” (2,546 training, 101 validation as test), and “zebra” (1,916 training, 85 validation as test)—all uniformly resized to  $512 \times 512$  resolution to ensure comparability. A consistent target-aware occlusion protocol was implemented across all datasets, automatically generating masks from target maps to restrict occlusions exclusively to foreground areas, with coverage constrained to  $\sim 40\%$  of object regions during both training and inference phases to preserve contextual information while necessitating complex structural reasoning.

### 4.2. Experimental Setup

**Implementation Details.** All experiments were conducted on an Ubuntu 20.04 system equipped with an Intel Xeon Platinum 8358P CPU and an NVIDIA GeForce RTX 4090 GPU (24 GB VRAM). The framework was implemented in PyTorch 1.10.0 with CUDA 11.3 support. Training spanned 50 epochs with a batch size of 4, constrained by available computational resources. Optimization employed Adam with a learning rate of  $2 \times 10^{-4}$ , resulting in approximately 0.5 hours of total training time on the specified hardware. We adopted a two-stage training protocol: First, the ObjectImagingModule was pretrained exclusively using  $\mathcal{L}_{\text{recon}}$  to generate semantically structured intermediate representations. This plug-and-play module was subsequently frozen and integrated across all four experimental configurations. Second, the Structural Refinement Module (SRM) and Geometric Detail Reconstruction Module (GDRM) were trained using  $\mathcal{L}_{\text{perc}}$  and  $\mathcal{L}_{\text{style}}$  to enhance semantic coherence and stylistic fidelity. This secondary optimization (implemented solely for preliminary validation in Experiment 1) maintained the ObjectImagingModule’s parameters fixed. Full implementation code is available at: <https://github.com/WYH302/WuYonghao.git>.

**Baseline.** To rigorously evaluate the efficacy of our proposed method, we benchmark against a representative spectrum of state-of-the-art inpainting approaches selected through a multi-faceted lens. Our criteria prioritize comprehensive coverage of methodological evolution, spanning from classical exemplar-based techniques to cutting-edge generative models, while ensuring architectural diversity across diffusion, transformer, and GAN-based paradigms. The evaluation suite begins with foundational exemplar-based methods: Criminisi [18], representing classical non-local patch synthesis, establishes a performance baseline for traditional non-deep-learning approaches and highlights inherent limitations in complex structural recovery. Its optimized counterpart, PatchMatch [78], provides critical insights into computational efficiency trade-offs through accelerated nearest-neighbor matching. Transitioning to modern deep learning, AOT-GAN [79] is included for its attention-driven, long-range dependency modeling via dilated convolutions—directly addressing holistic scene coherence challenges central to our work. Edge-Connect [56] offers a strategic comparative lens as a two-stage edge-guided model, enabling explicit evaluation of structural prior utilization against our coarse-to-fine refinement paradigm. The hybrid methodology of MISF [80] tests multi-scale feature interaction between traditional and deep components against our biologically inspired framework. Finally, contemporary diffusion models LaMa [81] and RePaint [41] are incorporated as cutting-edge references, with LaMa validating spectral processing choices and RePaint contrasting stochastic refinement against our deterministic pipeline. All baselines underwent five independent runs with randomized initializations, utilizing official implementations and pre-trained models where available.

**Evaluation metrics.** We employed four widely used metrics to quantify inpainting performance: (1) *SSIM* (Structural Similarity Index Measure), which assesses structural similarity between predictions and ground truth (higher is better); (2) *PSNR* (Peak Signal-to-Noise Ratio), measuring pixel-wise reconstruction fidelity (higher is better); (3) *MAE* (Mean Absolute Error), which measures average absolute pixel deviation (lower is better); and (4) *LPIPS* [82], a learned perceptual metric based on deep features (lower is better).

#### 4.3. Preliminary Theoretical Verification

To isolate and validate the core contribution of our work—the Specific Object-of-Interest Imaging (SIOI) module—we first conducted a controlled experiment using a simplistic subsequent inpainting network (Stage II:

SRM+GDRM). It is crucial to emphasize that this inpainting network is intentionally simplistic and is not the focus of our innovation. Its sole purpose is to serve as a stable and transparent baseline to demonstrate that the high-quality output is primarily attributable to the superior structural and semantic priors generated by the SIOI module (Stage I).

Unlike conventional image inpainting methods, our model eliminates the need for additional manually annotated corruption masks and is capable of automatically identifying and inpainting the corrupted regions of the target. We deliberately retained some black borders to demonstrate that the model does not solely rely on the color black to identify corrupted regions. As shown in Table 2 and Fig. 6, even with this simple network, the pipeline achieves exceptional performance on the Teapot dataset. This result provides foundational evidence that the SIOI module successfully accomplishes its design goal: to extract a clean, well-defined, and structurally sound representation of the target object from a complex and occluded scene. This output serves as an ideal input for anydownstream inpainting task, thereby validating the SIOI module’s efficacy as a standalone component.

Table 2: Preliminary Theoretical Verification on the teapot dataset (mean  $\pm$  std over five runs).  $\uparrow$  means higher is better, and  $\downarrow$  means lower is better.

Evaluation metrics	SSIM $\uparrow$	PSNR $\uparrow$	MAE $\downarrow$	LPIPS $\downarrow$
Experimental values	$0.98 \pm 0.02$	$33.86 \pm 0.38$	$1.61 \pm 0.18$	$0.02 \pm 0.01$

#### 4.4. Generalized empirical evaluation—Quantitative comparisons

Having established the standalone effectiveness of the SIOI module, we now evaluate its primary value proposition: its utility as a universal, plug-and-play front-end that can enhance diverse, off-the-shelf inpainting models. We integrated our SIOI module with a wide spectrum of state-of-the-art methods, spanning from classical algorithms to modern deep learning approaches. To ensure a fair comparison, all baseline methods were re-evaluated using a consistent object-level evaluation protocol, where their outputs were multiplied by corresponding object masks prior to quantitative analysis.

As summarized in Table 3, the SIOI module consistently enables significant performance improvements across all evaluation metrics. The key observation is not the absolute performance of any single model, but the transformative gain achieved by prepending SIOI. For instance, SIOI enables Criminisi to

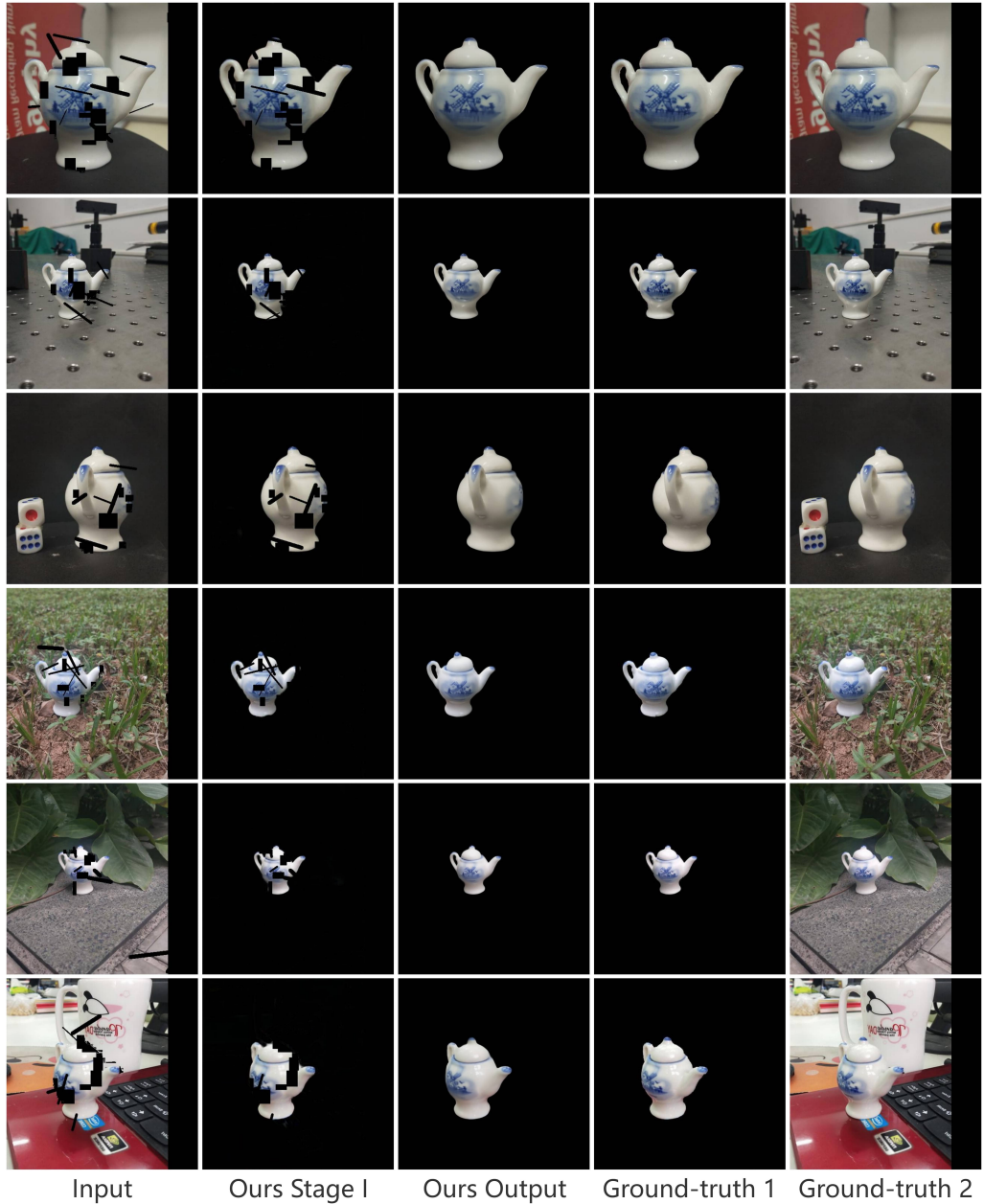


Figure 6: Preliminary Theoretical Verification of exemplar inpainting results (teapot dataset).

achieve a PSNR of 31.552 dB, a 7 dB improvement over the vanilla version. More notably, SIOI boosts LaMa to a staggering 45.222 dB PSNR and 0.0023 LPIPS, significantly surpassing all other methods. The improvements are especially pronounced on the Teapot dataset, where SIOI+LaMa achieves near-perfect reconstruction (SSIM: 0.9973, LPIPS: 0.0023). These results demonstrate that SIOI is not merely complementary but revolutionary, allowing both traditional and modern algorithms to transcend their inherent limitations by providing a purified, object-centric input. Regarding computational efficiency, SIOI acts as a generic adapter, effectively bridging the gap between holistic image processing and efficient object-centric reconstruction.

Across multiple datasets, models incorporating SIOI consistently achieve superior results in SSIM, PSNR, MAE, and LPIPS metrics compared to those without SIOI. Furthermore, models employing SIOI exhibit significantly enhanced perceptual quality. These results substantiate the effectiveness of SIOI in achieving high-fidelity reconstruction of objects with complex textures. Additionally, the object-centric imaging paradigm facilitates consistent separation of target objects across diverse backgrounds. Regarding computational efficiency, SIOI reduces redundant computations by concentrating processing resources on target regions, thereby accelerating inference while maintaining reconstruction quality.

#### 4.5. Generalized empirical evaluation—Qualitative comparisons

Qualitative results further corroborate the role of SIOI as a powerful pre-processing stage. By providing a clean, background-suppressed, and structurally coherent representation of the target object, SIOI enables even conventional algorithms to produce more semantically consistent and visually plausible results. Fig. 7, Fig. 8, Fig. 9, Fig. 10, Fig. 11, Fig. 12, Fig. 13, Fig. 14, presents qualitative results that highlight characteristic behaviors and failure modes of the benchmark models. Criminisi [18] fundamentally lacks semantic understanding in its non-local patch matching, leading to severe structural discontinuities and semantically inconsistent textures in complex scenes. Similarly, PatchMatch [78] remains constrained by hand-crafted features and low-level metrics, failing to capture high-level semantics or global coherence, which results in visible patch artifacts—a byproduct of its localized/static patch-level processing that becomes evident under gradient-rich lighting and on non-rigid surfaces. AOT-GAN [79] exhibits jagged artifacts and discontinuous textures in complex regions, these failures

Table 3: Experimental Results for Different Datasets and Models,  $\uparrow$  means higher is better, and  $\downarrow$  means lower is better.

Datasets	Model	SSIM $\uparrow$	PSNR $\uparrow$	MAE $\downarrow$	LPIPS $\downarrow$
<b>teapot</b>	Criminisi	0.9415	24.597	3.5517	0.0965
	PatchMatch	0.9212	21.219	5.4619	0.1263
	Edge-Connect	0.9457	25.095	3.3687	0.0908
	AOT-GAN	0.9487	25.329	3.2564	0.0863
	MISF	0.9370	24.871	3.7130	0.1178
	LaMa	0.9524	25.534	3.1024	0.0833
	RePaint	0.9330	24.037	4.1087	0.1141
	SIOI+Criminisi	0.9841	31.552	0.7396	0.0246
	SIOI+PatchMatch	0.9752	25.912	1.7894	0.0408
	SIOI+Edge-Connect	0.9795	32.378	0.8364	0.0299
	SIOI+AOT-GAN	0.9248	36.940	1.0471	0.0094
	SIOI+MISF	0.9739	33.487	1.0541	0.0674
	SIOI+LaMa	0.9973	45.222	0.1119	0.0023
	SIOI+RePaint	0.9712	28.599	1.6907	0.0645
<b>elephant</b>	Criminisi	0.9671	32.615	1.3453	0.0262
	PatchMatch	0.9596	28.643	2.1005	0.0441
	Edge-Connect	0.9562	31.958	1.7455	0.0423
	AOT-GAN	0.8416	27.653	4.9353	0.0608
	MISF	0.8472	23.789	5.2913	0.1908
	LaMa	0.9236	26.059	2.9596	0.0949
	RePaint	0.8624	23.690	5.1769	0.1676
	SIOI+Criminisi	0.9774	33.152	0.8312	0.0190
	SIOI+PatchMatch	0.9721	29.327	1.3736	0.0325
	SIOI+Edge-Connect	0.9636	30.693	1.2479	0.0448
	SIOI+AOT-GAN	0.9341	34.691	1.4350	0.0243
	SIOI+MISF	0.8883	29.070	3.4237	0.1848
	SIOI+LaMa	0.9786	34.706	0.6523	0.0140
	SIOI+RePaint	0.9102	28.956	3.2348	0.1489
<b>giraffe</b>	Criminisi	0.9721	29.962	1.5050	0.0184
	PatchMatch	0.9653	27.671	2.3031	0.0368
	Edge-Connect	0.9678	29.914	1.6754	0.0280
	AOT-GAN	0.9109	26.742	4.1489	0.0388
	MISF	0.8998	23.505	4.6733	0.1208
	LaMa	0.9424	25.732	2.5901	0.0670
	RePaint	0.9079	23.563	4.5075	0.1096
	SIOI+Criminisi	0.9788	29.824	1.1000	0.0170
	SIOI+PatchMatch	0.9734	26.327	1.7493	0.0306
	SIOI+Edge-Connect	0.9676	27.527	1.6295	0.0382
	SIOI+AOT-GAN	0.8741	30.861	2.3573	0.0350
	SIOI+MISF	0.9325	27.270	3.0461	0.1215
	SIOI+LaMa	0.9796	31.023	0.9491	0.0129
	SIOI+RePaint	0.9465	27.109	2.8830	0.0992
<b>zebra</b>	Criminisi	0.9677	27.598	2.2333	0.0236
	PatchMatch	0.9262	22.627	4.1497	0.0857
	Edge-Connect	0.9588	27.891	3.1040	0.0263
	AOT-GAN	0.8451	22.399	9.6206	0.0486
	MISF	0.8583	21.409	8.2618	0.1596
	LaMa	0.9331	24.284	3.7468	0.0684
	RePaint	0.8677	21.544	8.0205	0.1499
	SIOI+Criminisi	0.9750	27.389	1.6940	0.0211
	SIOI+PatchMatch	0.9675	24.691	2.4553	0.0365
	SIOI+Edge-Connect	0.9632	26.089	2.2360	0.0387
	SIOI+AOT-GAN	0.9070	28.025	3.2725	0.0527
	SIOI+MISF	0.8960	24.048	6.2437	0.1556
	SIOI+LaMa	0.9772	28.811	1.3896	0.0144
	SIOI+RePaint	0.9130	24.309	5.9439	0.1365

stem from its use of dilated convolutions for feature aggregation. Edge-Connect [56], while effective in many cases, suffers from visible spatial misalignment due to its over-reliance on imperfect Canny edges, which do not correspond to perceptually relevant structures and disrupt spatial coherence in repetitive textures (e.g., grass). MISF [80] produces overly smooth, artificial-looking edges and illumination inconsistencies, resulting from its multi-scale regularization and strong smoothing priors as well as incompatible traditional and deep feature interactions. LaMa [81] over-smooths detailed regions and produces blurry or insufficiently sharp outputs despite its efficient Fourier-based design. RePaint [41] often yields overly smooth or blurry outputs with incongruous textures due to its slow. Without using our method, existing methods exhibit characteristic failures due to background interference and a lack of object-level understanding, resulting in color and texture details related to the background that are completely inconsistent with their original objects.

In contrast, the integration of the SIOI module consistently guides the inpainting focus, resulting in improved edge sharpness, texture consistency, and semantic coherence, regardless of the backend inpainting algorithm used. Experimental results across multiple object datasets show that our approach performs particularly well on rigid objects (e.g., teapots), while achieving relatively weaker results on non-rigid objects such as giraffes, zebras, and elephants. We attribute this difference to the higher morphological variability and structural complexity of non-rigid categories, which may require larger or more adaptive model parameters to adequately capture their semantic and textural characteristics. Preliminary observations suggest a potential linear relationship among semantic complexity, training data scale, and model parameter quantity—a phenomenon that merits further quantitative investigation in future work.

#### 4.6. Ablation Studies

In fact, a detailed ablation experiment has already been conducted above, So this is just a simple supplement to the Preliminary Theoretical Verification experiment, also conducted on the Teapot dataset. This experiment is based on the preliminary theoretical verification experiment. To evaluate the effectiveness of our methodology, we conducted ablation studies under identical experimental conditions. Key components were systematically removed, and the resulting imaging outcomes were comparatively analyzed to elucidate performance differences. As shown in Fig. 15.

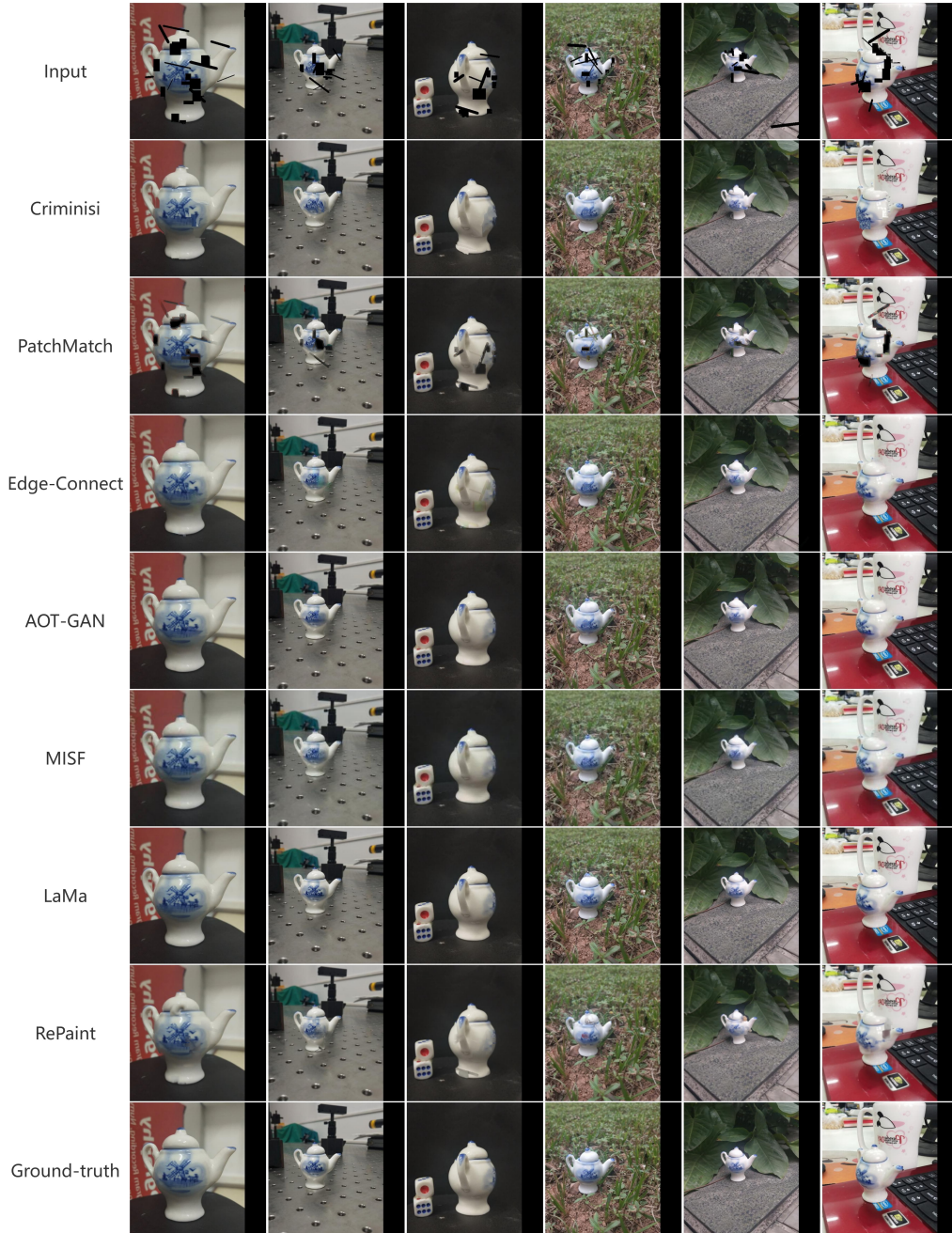


Figure 7: Qualitative comparison of exemplar inpainting results (teapot dataset).

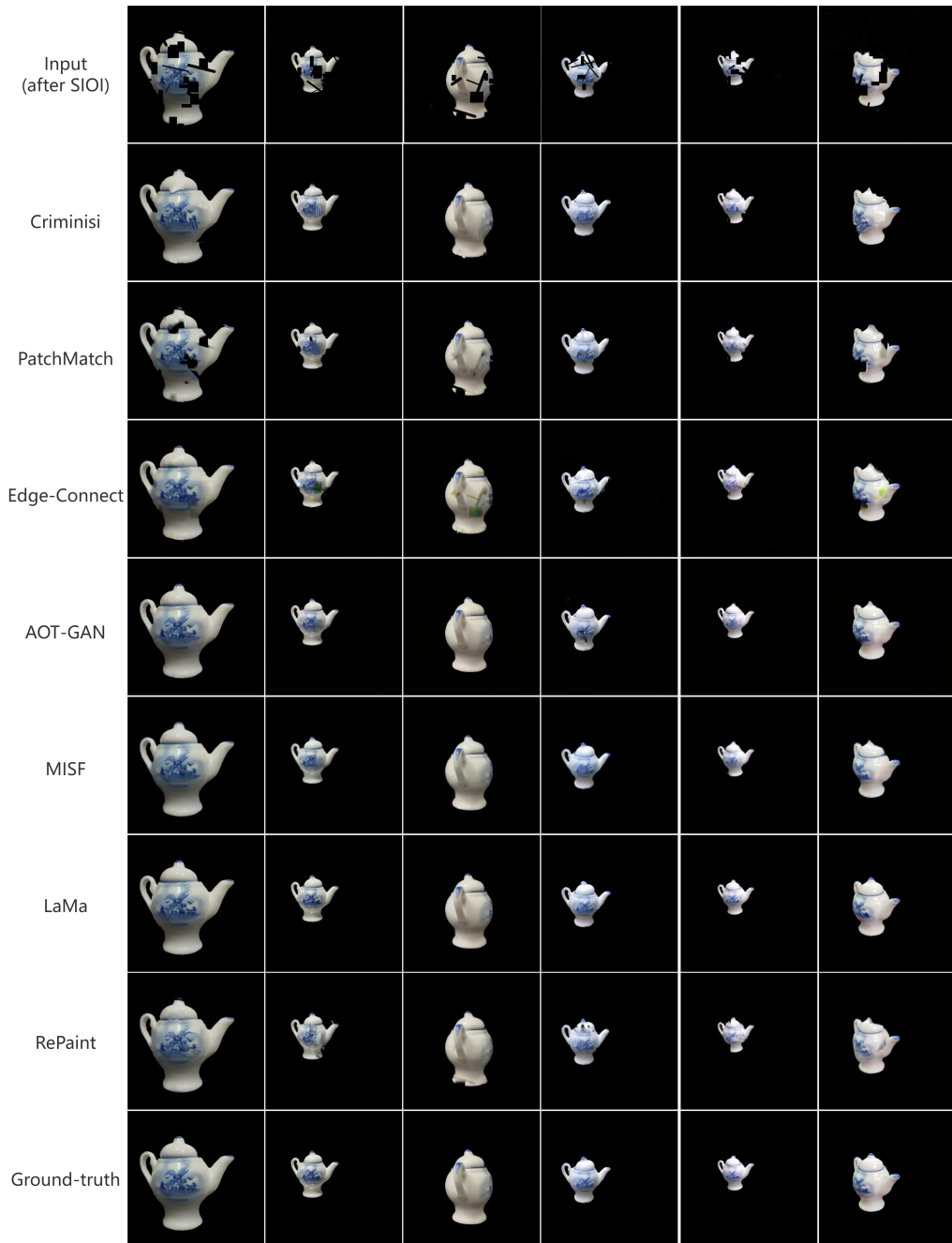


Figure 8: Qualitative comparison of exemplar SIOI inpainting results (teapot dataset).



Figure 9: Qualitative comparison of exemplar inpainting results (elephant dataset).

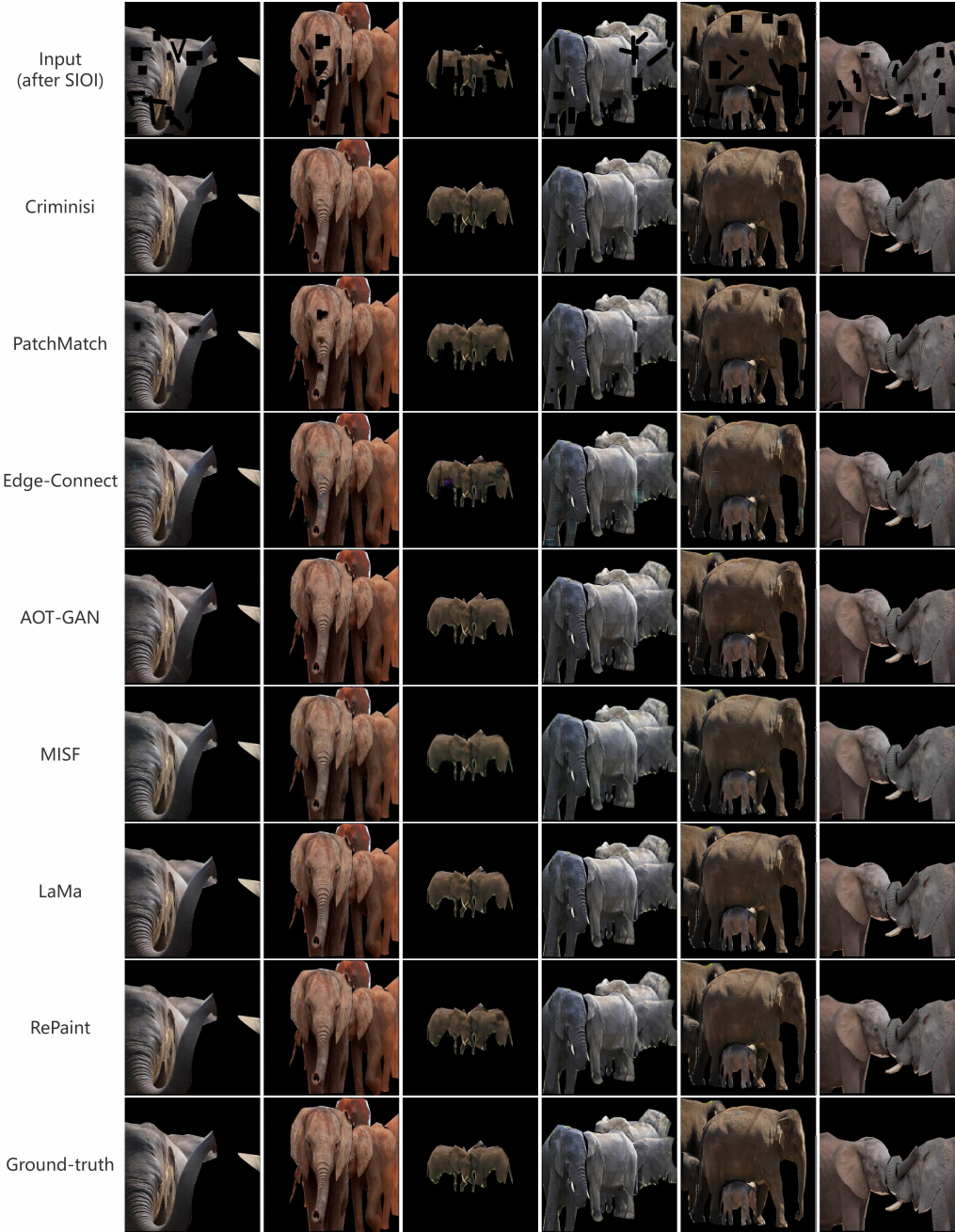


Figure 10: Qualitative comparison of exemplar SIOI inpainting results (elephant dataset).

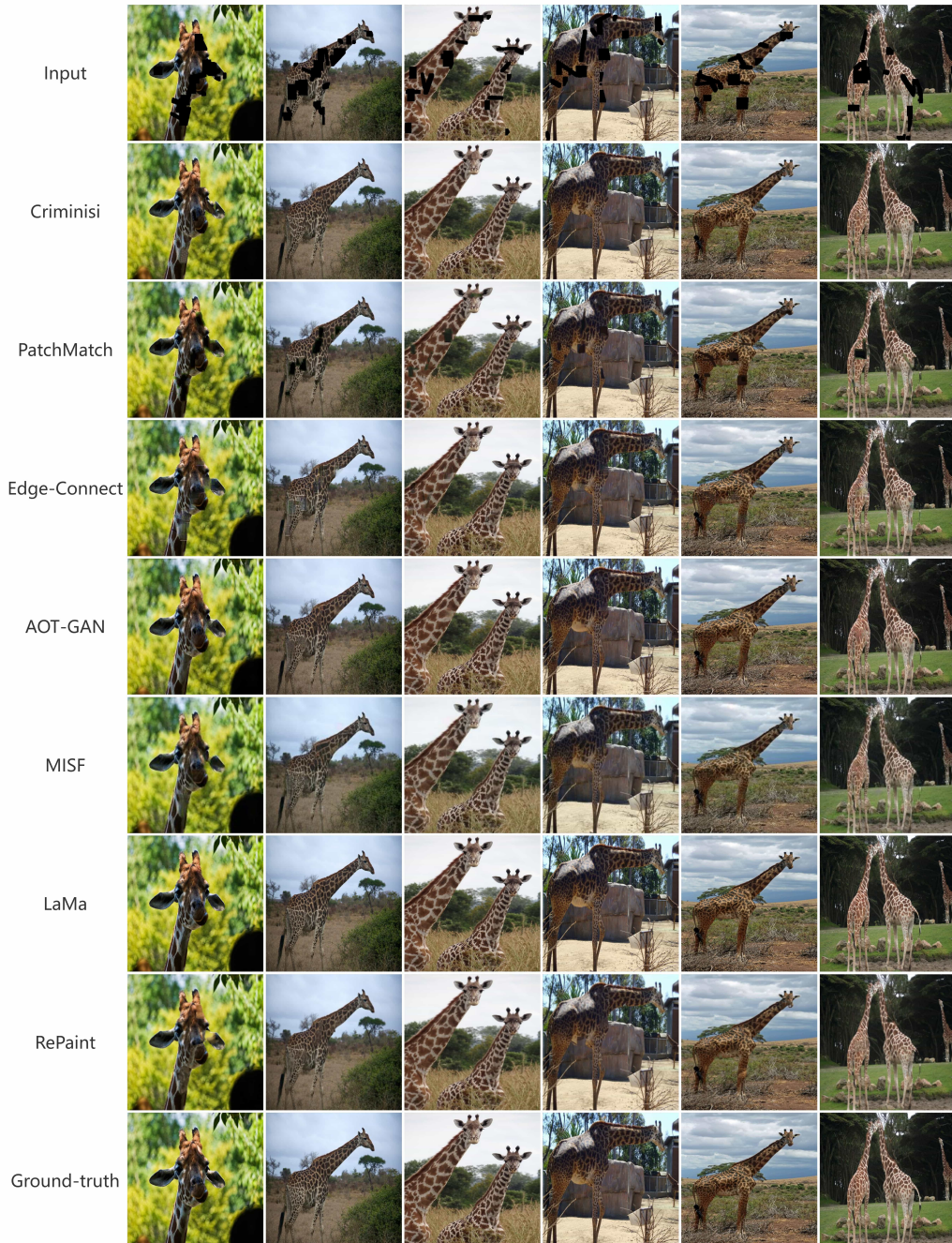


Figure 11: Qualitative comparison of exemplar inpainting results (giraffe dataset).

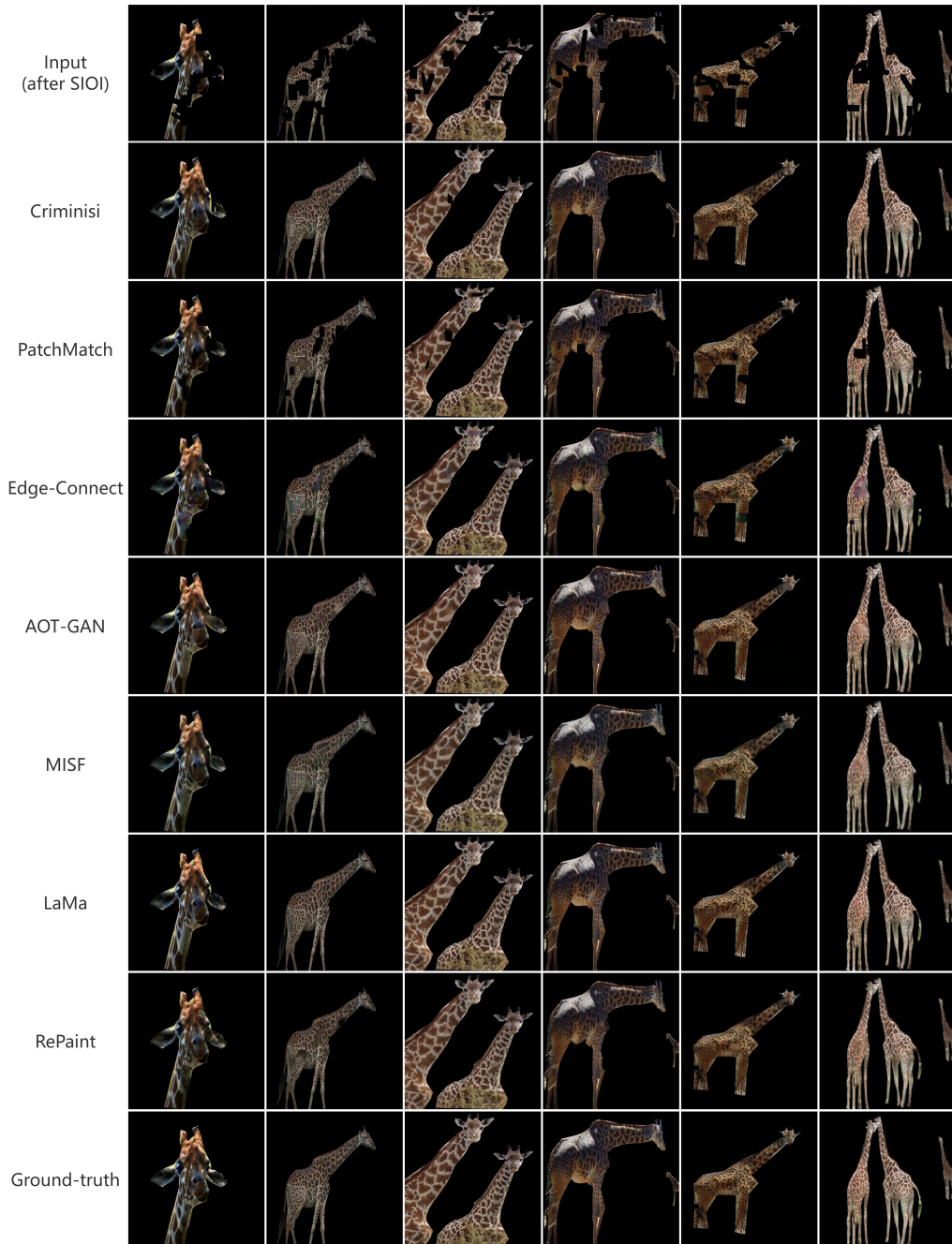


Figure 12: Qualitative comparison of exemplar SIOI inpainting results (giraffe dataset).

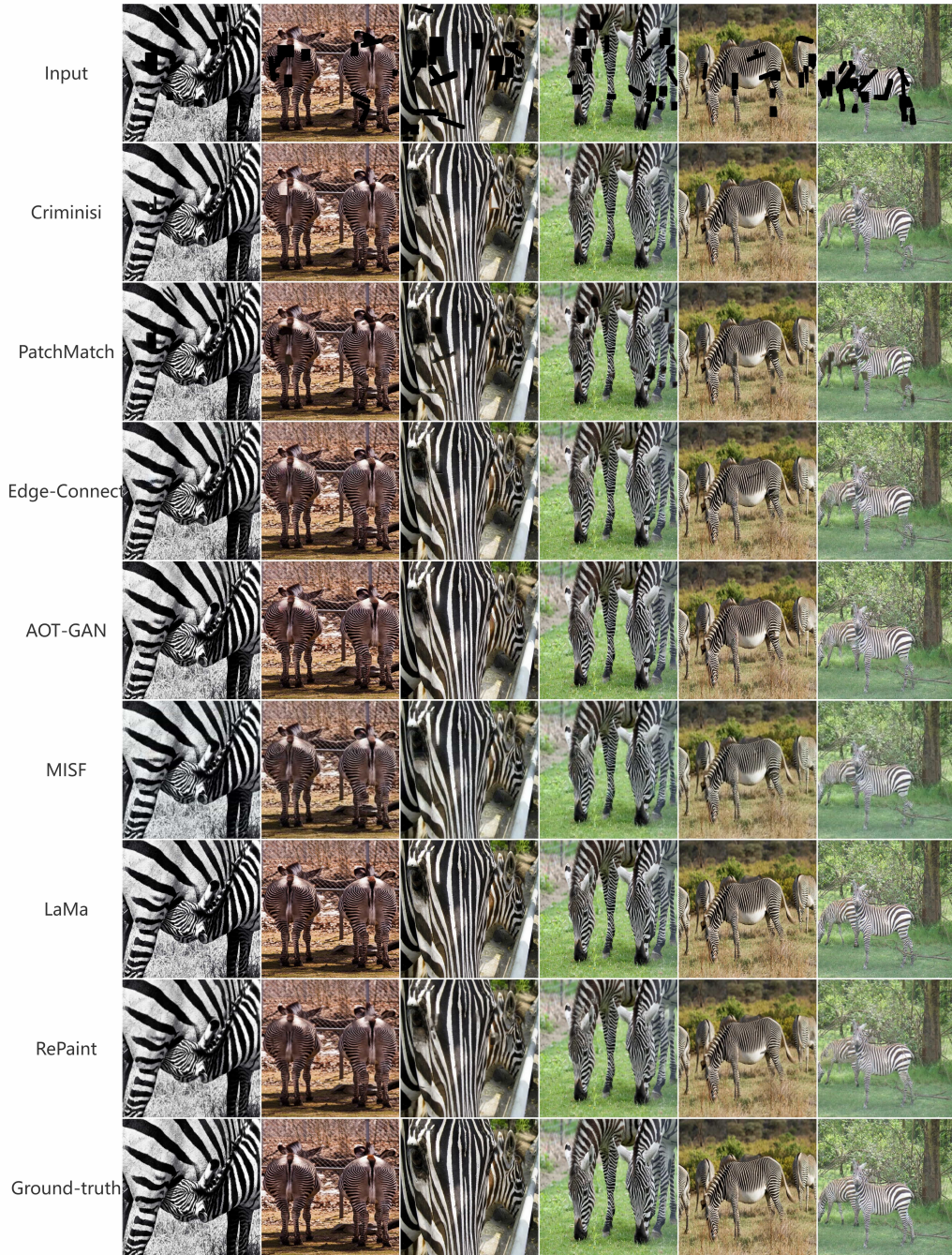


Figure 13: Qualitative comparison of exemplar inpainting results (zebra dataset).

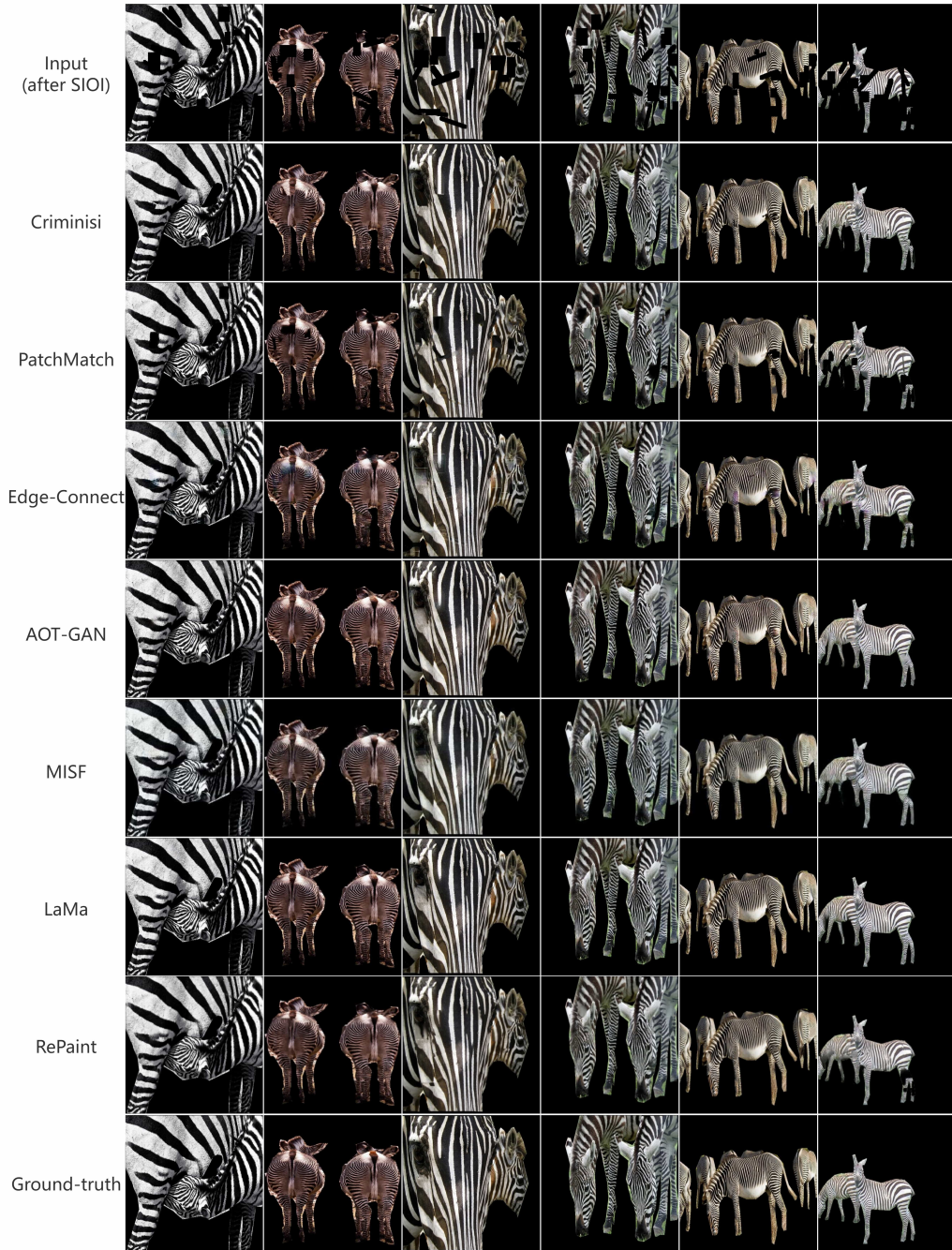


Figure 14: Qualitative comparison of exemplar SIOI inpainting results (zebra dataset).

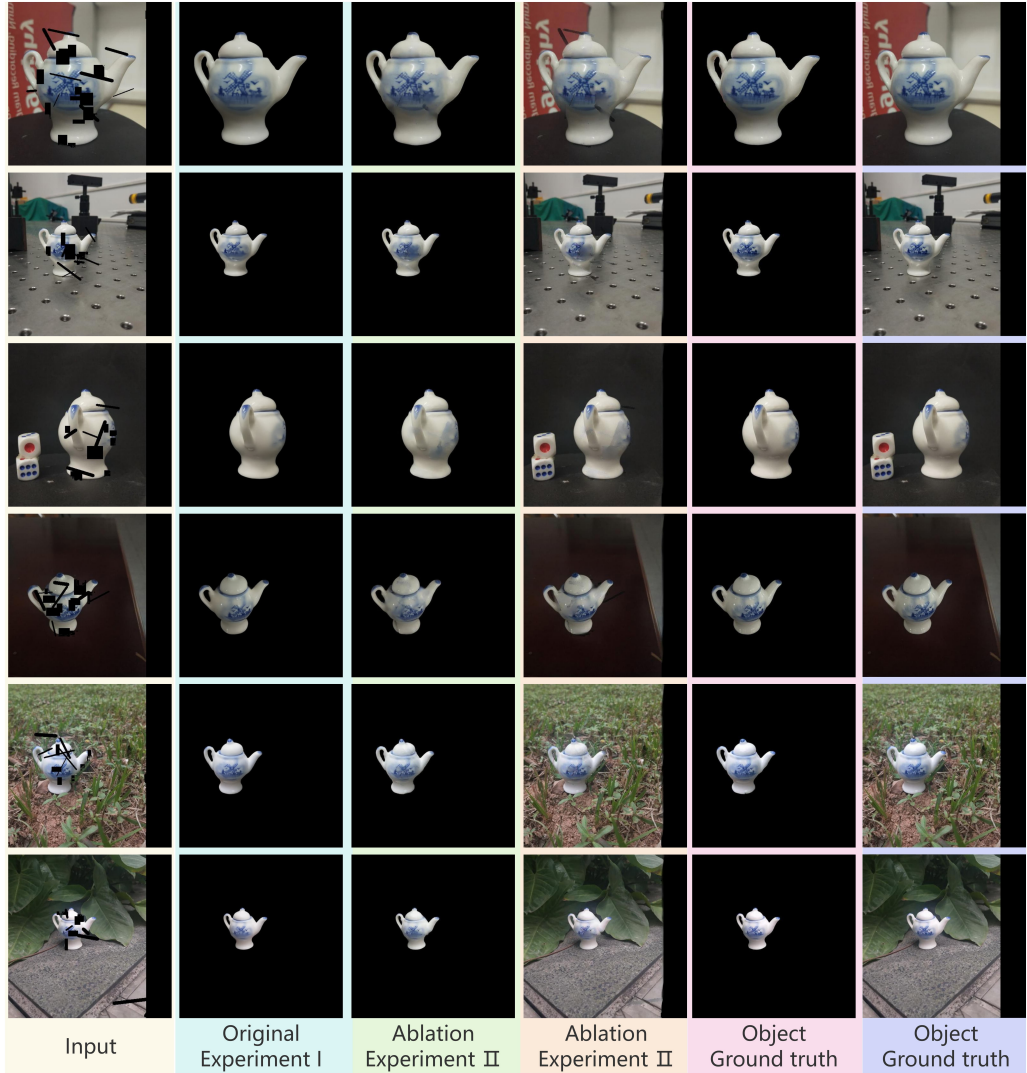


Figure 15: Illustration of ablation experiment.

**Ablation I:** In Ablation I, the state I network was removed while retaining the object-centric input–output pipeline. The corresponding results are presented in Tab. 4. The resulting model showed marginal superiority in certain quantitative metrics compared to the proposed method—SSIM (0.976 vs. 0.978), PSNR (33.95 dB vs. 33.86 dB), MAE (1.313 vs. 1.605), and LPIPS (0.017 vs. 0.018)—but these differences were statistically insignificant in terms of perceptual quality. However, subjective evaluation revealed compromised edge localization, manifested as jagged artifacts and global blurring. This degradation confirms the critical role of Stage I in achieving high structural precision. Furthermore, visual comparisons clearly demonstrated the superior inpainting quality achieved when Stage I was integrated. The marginal improvements observed in PSNR and MAE, despite perceptual and qualitative degradation, further highlight that such metrics can be misleading indicators of inpainting quality, as they from the loss function’s direct penalization of RGB deviations, do not consistently align with human perceptual judgment.

**Ablation II:** In Ablation II, the object-centric I/O was replaced with full-scene inputs. The model processed the entire image, including the extensive and complex background, which resulted in severe performance degradation. This represents the standard paradigm used by most existing methods, which our SIOI approach aims to supersede for object-centric tasks. Quantitative metrics showed substantial deterioration: SSIM: 0.964, PSNR: 29.43 dB, MAE: 2.085, LPIPS: 0.065. Visual inspection confirmed that this configuration yielded the poorest inpainting quality among all compared models. It exhibited pronounced detail loss, extensive artifacts throughout the restored regions, and markedly impaired image clarity. Furthermore, the model’s inability to effectively extract features, particularly from the edges of degraded regions, resulted in insufficient feature representation during inpainting. This shortfall directly led to blurry reconstruction and pervasive artifact generation. This ablation highlights the fundamental advantage of our object-first paradigm: it dramatically reduces the solution space by focusing computation exclusively on the target, thereby avoiding the pitfalls of whole-image processing.

In contrast to both ablated versions, the full model (with SIOI) achieved superior performance, delivering sharp edges, semantically coherent structures, and photorealistic textures. This provides compelling evidence that our two-stage pipeline, headed by the SIOI module, effectively addresses the bottlenecks of traditional inpainting by first resolving the "where and what" of the target object before addressing the "how" of its inpainting. The SIOI module acts as a powerful pre-processor that can be plugged into any

inpainting network to elevate its performance on object-centric tasks.

Table 4: Comparison of ablation study results on the Teapot dataset. (mean  $\pm$  std over five runs).  $\uparrow$  means higher is better, and  $\downarrow$  means lower is better.

Model	SSIM $\uparrow$	PSNR $\uparrow$	MAE $\downarrow$	LPIPS $\downarrow$
Origin	$0.98 \pm 0.01$	$33.86 \pm 0.38$	$1.61 \pm 0.08$	$0.02 \pm 0.01$
Ablation I	$0.98 \pm 0.01$	$33.95 \pm 0.19$	$1.31 \pm 0.06$	$0.02 \pm 0.01$
Ablation II	$0.96 \pm 0.01$	$29.43 \pm 0.25$	$2.09 \pm 0.15$	$0.07 \pm 0.02$

#### 4.7. Robustness Analysis

This experiment is based on the preliminary theoretical verification experiment, also conducted on the Teapot dataset. To evaluate the generalization ability of our method under challenging conditions, we conducted robustness experiments on the following scenarios:

- *Low illumination*: 50% reduced scene brightness
- *Small targets*: Objects occupying  $< 5\%$  image area
- *Gaussian noise*: Additive noise ( $\mu = 0, \sigma = 1$ )
- *Salt-and-pepper noise*: Impulse noise ( $p_{\text{salt}} = 0.01, p_{\text{pepper}} = 0.01$ )
- *Multi-object occlusion*: 3 instances
- *Motion blur*: Linear kernel with  $15 \times 15$  pixels

It should be noted that these challenging scenarios were not part of the training data. For qualitative assessment, two representative samples were selected per category. Quantitative evaluation was omitted due to the limited number of available samples for each specific condition, as illustrated in Fig. 16.

The qualitative results demonstrate the SIOI module’s notable robustness in several challenging conditions. It consistently maintained satisfactory target extraction performance under low illumination, small targets, salt-and-pepper noise, and motion blur. This resilience can be attributed to the module’s design principles: its spectral processing (FFC) is inherently robust to global illumination changes and motion artifacts, while its attentional mechanisms,

inspired by V4 cortical processing, enable it to amplify and track small or salient targets despite noise. Performance degradation emerged in scenarios with three or more coexisting objects, as the competition for attentional resources increased. This observation directly mirrors the biological phenomenon of attentional limitation described in Desimone and Duncan’s biased competition model [66], validating the bio-inspired nature of our approach even in its failure modes.

The most substantial degradation occurred under high-power Gaussian noise. This is a recognized challenge for feature-based attentional systems both in biological and artificial networks. The SIOI module’s reliance on gradient and frequency information for target selection makes it particularly susceptible to this type of non-structured, high-entropy noise, which overwhelms the salient features the module is designed to detect. This result precisely highlights the critical role and inherent vulnerability of the front-end SIOI module: its output quality is the foundational prior for all subsequent processing. This underscores the importance of our modular design—the failure is contained and diagnosed at the SIOI stage, preventing a cascading collapse of the entire system and clearly pointing to the component that requires improvement.

These findings provide a clear roadmap for evolving the SIOI module. Future work will focus on enhancing its robustness against unstructured noise, potentially by incorporating neuromorphic noise-adaptation mechanisms inspired by the auditory brainstem or retinal adaptive gain control. This will further solidify the SIOI module’s role as a robust, plug-and-play pre-processor for object-centric vision tasks.

In summary, the robustness analysis confirms that the SIOI module provides a reliable and highly effective object-specific prior across a wide spectrum of challenging conditions. Its performance profile—strong in structured degradation but susceptible to unstructured noise—precisely characterizes its operational envelope and offers valuable insights for its application and further development as a general-purpose biological vision-inspired front end.

## 5. Discussion

Image inpainting is a job without a standard answer and often leads to controversy, as shown in Fig. 17. We don’t even know if the black area should be an buffalo head or a zebra head. The same model, when the same image is input multiple times, will yield different results. And the work proposed in

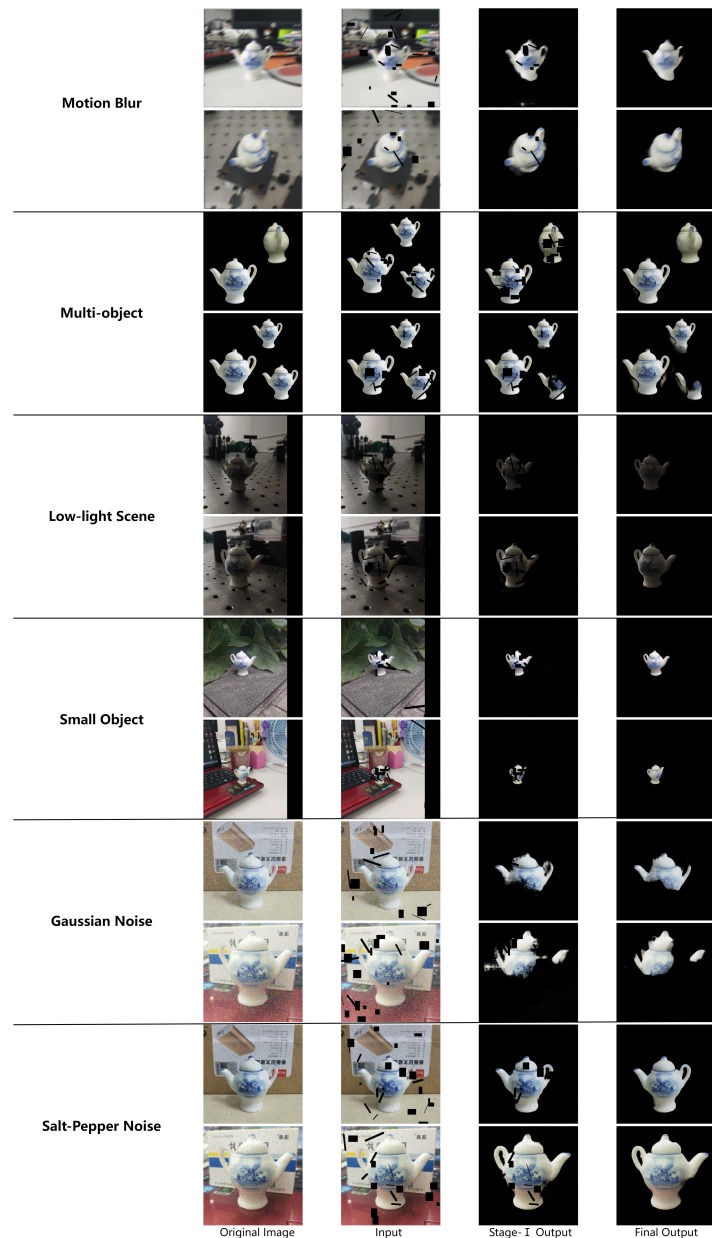


Figure 16: Illustration of robustness experiment.

this article can solve this problem. This work introduces Specific Object-of-Interest Imaging (SIOI)—a novel, bio-inspired paradigm that fundamentally rethinks the pipeline for object-centric visual computing tasks. Departing from conventional holistic processing, SIOI provides a plug-and-play front-end module that first isolates and enhances the target object, generating a refined structural and semantic prior that can be seamlessly integrated into any subsequent processing network. Our experimental validation demonstrates that incorporating the SIOI module consistently elevates the performance of diverse inpainting architectures. This is not a contest between inpainting models; rather, it is a demonstration that providing a high-quality, object-centric prior is a more impactful lever for improvement than designing yet another holistic inpainting network.



Figure 17: Misunderstand of image inpainting.

This approach aligns with the ventral pathway's "object-before-background" processing strategy, where attentional mechanisms in areas like V4 selectively amplify target features while suppressing irrelevant background clutter[83]. Our SIOI module computationally instantiates this principle, thereby mitigating the fundamental issue of information redundancy that plagues whole-image methods. Compared to GAN- or diffusion-based approaches that operate on the entire scene, our method avoids propagating errors from background regions by focusing computation on the target, akin to V4's role in contour integration and feature binding.

The robustness of the SIOI module under extreme conditions (e.g., low illumination, noise) further underscores its utility as a reliable pre-processor.

Its behavior is consistent with the object-based attention mechanism in biological vision, which dynamically modulates early visual areas (V1-V4) to maintain target salience amidst distraction. It is important to note that the performance of any subsequent model is contingent on the quality of the prior provided by SIOI. This dependency mirrors the dorsal-ventral synergy in the brain, where spatial localization guides object recognition. This highlights that advancing object-level pre-processing is a critical frontier in itself.

We emphasize that the inpainting network presented in Stage II serves primarily as a proof-of-concept vehicle to validate the efficacy of the SIOI prior. Our architecture may not represent the ultimate performance ceiling, and that future researchers may develop superior networks. The paramount innovation of this work is not this specific network, but the SIOI paradigm itself. This paradigm shift—from direct holistic inpainting to object-first prior generation—is our central contribution. The generalization of the SIOI module is inherently tied to the semantic definition of a "specific object." This is not merely a limitation but a defining characteristic and a research opportunity. But we must frankly admit that the generalization of this technology is not strong due to its focus on specific objects. And each semantic object represents a type of dataset, which also requires retraining the object imaging network. For example, whether cat is an object, or is it divided into jungle cat *felis chaus*, sand cat *felis Margarita*, black foot cat *felis nigripes*, and wild cat *felis silvestris* (which is also more refined as a specific object) needs further research. The module's performance can be scaled and specialized, offering a practical pathway for technology transfer, allowing the SIOI paradigm to be precisely tailored to application-specific needs.

Future work will explore integrating prefrontal-cortex-like task-driven modulation to enable dynamic reconfiguration of the SIOI module for different object categories and end goals, advancing toward truly adaptive and biologically plausible computational vision systems.

## 6. Conclusion

In conclusion, this work proposes Specific Object-of-Interest Imaging (SIOI) as a novel, bio-inspired pre-processing paradigm for object-centric visual tasks. SIOI operates by first isolating and enhancing the target object, providing a high-fidelity prior that dramatically improves the performance of subsequent vision modules. Extensive experiments confirm that the SIOI module is a powerful, plug-and-play front-end that consistently improves var-

ious inpainting models by suppressing background interference and providing a coherent object-centric prior. Its design is grounded in the "object-first" processing hierarchy of the ventral visual pathway, offering a computational solution to the problem of information redundancy. The framework demonstrates strong robustness across challenging conditions, reflecting the resilience of biological attentional systems. Limitations arise from reliance on initial object generation, which may impair boundary guidance. We envision the SIOI paradigm extending beyond inpainting to benefit a wide array of object-centric applications, including segmentation, detection, and video tracking, wherever suppressing background clutter and focusing computational resources on the target is paramount. Future work will explore task-driven modulation and fMRI validation, advancing toward biologically adaptive imaging and broader applications in neuroimaging and perceptual assistance.

## References

- [1] M. Bertalmio, G. Sapiro, V. Caselles, C. Ballester, Image inpainting, in: Proceedings of the 27th annual conference on Computer graphics and interactive techniques, 2000, pp. 417–424, doi:<https://doi.org/10.1145/344779.344972>.
- [2] A. Bugeau, M. Bertalmío, V. Caselles, G. Sapiro, A comprehensive framework for image inpainting, *IEEE transactions on image processing* 19 (10) (2010) 2634–2645, doi:<https://doi.org/10.1109/TIP.2010.2049240>.
- [3] C. Guillemot, O. Le Meur, Image inpainting: Overview and recent advances, *IEEE signal processing magazine* 31 (1) (2013) 127–144, doi:<https://doi.org/10.1109/MSP.2013.2273004>.
- [4] J. Yu, Z. Lin, J. Yang, X. Shen, X. Lu, T. S. Huang, Generative image inpainting with contextual attention, in: Proceedings of the IEEE conference on computer vision and pattern recognition, 2018, pp. 5505–5514, doi:<https://doi.org/10.48550/arXiv.1801.07892>.
- [5] O. Elharrouss, N. Almaadeed, S. Al-Maadeed, Y. Akbari, Image inpainting: A review, *Neural Processing Letters* 51 (2) (2020) 2007–2028, doi:<https://doi.org/10.1007/s11063-019-10163-0>.

Table 5: Extended Mathematical Notation Guide with Biological Correlations

Symbol	Mathematical Definition	Biological Mechanism	Network Implementation
$\Gamma$	Target-sensitive measurement matrix: $\Gamma k \approx \sum_{m=1}^M (\Gamma \omega_m) \otimes k_m$	LGN attentional filtering	SIOI spectral filtering
$k$	Scene tensor: $k \in \mathbb{R}^{H \times W \times C}$	Retinal photoreceptor output encoding	SIOI degraded input (Stage I)
$\otimes$	Diffeomorphic operator: $(\Gamma \omega_m) \otimes k_m$	Foveal cortical magnification	FFCModule feature warping
$\xi_j$	Orthogonal feature basis: $\xi_j \in \mathbb{R}^D$	V1 simple cell orientation responses	Multi-scale encoder features in SIOI
$\omega_m$	Feature weights: $\omega_m \rightarrow \delta_{m\mu}$	Neural resource allocation	Attention weights
$k_i$	Latent object tensor: $k_i \in \mathbb{R}^{h_i \times w_i \times C}$	IT cortex semantic object representation	Target object map (Stage I output)
$\phi$	Projection operator: $\phi = I - P_{\text{bg}}$	Dorsal pathway spatial suppression	TRNet background suppression
$D_{KL}$	Kullback–Leibler divergence: $D_{KL}(P\ Q) = \sum_i P_i \log \frac{P_i}{Q_i}$	Neural coding efficiency optimization	Loss function convergence
$\mathcal{F}$	Spectral feature map: $\mathcal{F}' = \text{IFFT2}(\text{Conv}_{\text{freq}}(\text{FFT2}(\mathcal{F})))$	V1–V4 spatial frequency processing	FFCModule operations in bottleneck
$\mathcal{L}_{\text{total}}$	Composite loss: $\mathcal{L}_{\text{total}} = \lambda_1 \mathcal{L}_{\text{recon}} + \lambda_2 \mathcal{L}_{\text{perc}} + \lambda_3 \mathcal{L}_{\text{style}}$	Prefrontal cortex task-driven modulation	Phased training strategy

- [6] Z. Qin, Q. Zeng, Y. Zong, F. Xu, Image inpainting based on deep learning: A review, *Displays* 69 (2021) 102028, doi:<https://doi.org/10.1016/j.displa.2021.102028>.
- [7] H. Xiang, Q. Zou, M. A. Nawaz, X. Huang, F. Zhang, H. Yu, Deep learning for image inpainting: A survey, *Pattern Recognition* 134 (2023) 109046, doi:<https://doi.org/10.1016/j.patcog.2022.109046>.
- [8] R. A. Yeh, C. Chen, T. Yian Lim, A. G. Schwing, M. Hasegawa-Johnson, M. N. Do, Semantic image inpainting with deep generative models, in: *Proceedings of the IEEE conference on computer vision and pattern recognition*, 2017, pp. 5485–5493, doi:<https://doi.org/10.48550/arXiv.1607.07539>.
- [9] T. Yu, R. Feng, R. Feng, J. Liu, X. Jin, W. Zeng, Z. Chen, Inpaint anything: Segment anything meets image inpainting, *arXiv preprint arXiv:2304.06790* doi:<https://doi.org/10.48550/arXiv.2304.06790> (2023).
- [10] H. Wang, J. Yang, J. Zhou, Harmony score-guided inpainting: Iterative refinement for seamless image inpainting, *Neurocomputing* (2025) 131001 doi:<https://doi.org/10.1016/j.neucom.2025.131001>.
- [11] Z. Zhang, F. Cai, Q. Zhou, Y. Ding, Sqfill: Joint spatial and spectral learning for high-fidelity image inpainting, *Neurocomputing* (2025) 130414 doi:<https://doi.org/10.1016/j.neucom.2025.130414>.
- [12] T. Liu, L. Liao, D. Chen, J. Xiao, Z. Wang, C.-W. Lin, S. Satoh, Transref: Multi-scale reference embedding transformer for reference-guided image inpainting, *Neurocomputing* 632 (2025) 129749, doi:<https://doi.org/10.48550/arXiv.2306.11528>.
- [13] W. Lu, H. Zhao, X. Jiang, X. Jin, Y.-L. Yang, K. Shi, Do inpainting yourself: Generative facial inpainting guided by exemplars, *Neurocomputing* 617 (2025) 128996, doi:<https://doi.org/10.48550/arXiv.2202.06358>.
- [14] Q. Mao, J. Li, H. Zhou, P. Kar, A. G. Bellotti, Aldii: Adaptive learning-based document image inpainting to enhance the handwritten chinese character legibility of human and machine, *Neurocomputing* 616 (2025) 128897, doi:<https://doi.org/10.1016/j.neucom.2024.128897>.

- [15] J. Liu, H. Cheng, S. Wang, F. Zhao, M. Li, Nerf dynamic scene reconstruction based on motion, semantic information and inpainting, *Neurocomputing* 630 (2025) 129653, doi:<https://doi.org/10.1016/j.neucom.2025.129653>.
- [16] T. F. Chan, S. H. Kang, J. Shen, Total variation denoising and enhancement of color images based on the cb and hsv color models, *Journal of Visual Communication and Image Representation* 12 (4) (2001) 422–435, doi:<https://doi.org/10.1006/jvci.2001.0491>.
- [17] D. Tschumperlé, R. Deriche, Vector-valued image regularization with pdes: A common framework for different applications, *IEEE transactions on pattern analysis and machine intelligence* 27 (4) (2005) 506–517, doi:<https://doi.org/10.1109/TPAMI.2005.87>.
- [18] A. Criminisi, P. Pérez, K. Toyama, Region filling and object removal by exemplar-based image inpainting, *IEEE Transactions on image processing* 13 (9) (2004) 1200–1212, doi:<https://doi.org/10.1109/TIP.2004.833105>.
- [19] A. A. Efros, T. K. Leung, Texture synthesis by non-parametric sampling, in: *Proceedings of the seventh IEEE international conference on computer vision*, Vol. 2, IEEE, 1999, pp. 1033–1038, doi:<https://doi.org/10.1109/ICCV.1999.790383>.
- [20] Y. Wexler, E. Shechtman, M. Irani, Space-time completion of video, *IEEE Transactions on pattern analysis and machine intelligence* 29 (3) (2007) 463–476, doi:<https://doi.org/10.1109/TPAMI.2007.60>.
- [21] I. Drori, D. Cohen-Or, H. Yeshurun, *Fragment-based image completion*, in: *ACM SIGGRAPH 2003 Papers*, SIGGRAPH '03, Association for Computing Machinery, New York, NY, USA, 2003, p. 303–312. doi: [10.1145/1201775.882267](https://doi.org/10.1145/1201775.882267).  
URL <https://doi.org/10.1145/1201775.882267>
- [22] J. Hays, A. A. Efros, Scene completion using millions of photographs, *ACM Transactions on graphics (TOG)* 26 (3) (2007) 4–es, doi:<https://doi.org/10.1145/1276377.1276382>.
- [23] A. Newson, A. Almansa, M. Fradet, Y. Gousseau, P. Pérez, Video inpainting of complex scenes, *Siam journal on imaging sciences* 7 (4) (2014) 1993–2019, doi:<https://doi.org/10.1137/140954933>.

- [24] D. Pathak, P. Krahenbuhl, J. Donahue, T. Darrell, A. A. Efros, Context encoders: Feature learning by inpainting, in: Proceedings of the IEEE conference on computer vision and pattern recognition, 2016, pp. 2536–2544, doi:<https://doi.org/10.48550/arXiv.1604.07379>.
- [25] T. Yu, Z. Guo, X. Jin, S. Wu, Z. Chen, W. Li, Z. Zhang, S. Liu, Region normalization for image inpainting, in: Proceedings of the AAAI conference on artificial intelligence, Vol. 34, 2020, pp. 12733–12740, doi:<https://doi.org/10.48550/arXiv.1911.10375>.
- [26] H. Liu, B. Jiang, Y. Song, W. Huang, C. Yang, Rethinking image inpainting via a mutual encoder-decoder with feature equalizations, in: European conference on computer vision, Springer, 2020, pp. 725–741, doi:<https://doi.org/10.48550/arXiv.2007.06929>.
- [27] N. Kumar, T. Meenpal, Encoder-decoder-based cnn model for detection of object removal by image inpainting, Journal of Electronic Imaging 32 (4) (2023) 042110–042110, doi:<http://dx.doi.org/10.1117/1.JEI.32.4.042110>.
- [28] S. Iizuka, E. Simo-Serra, H. Ishikawa, Globally and locally consistent image completion, ACM Transactions on Graphics (ToG) 36 (4) (2017) 1–14, doi:<https://doi.org/10.1145/3072959.3073659>.
- [29] Y. Wang, X. Tao, X. Qi, X. Shen, J. Jia, Image inpainting via generative multi-column convolutional neural networks, Advances in neural information processing systems 31, doi:<https://doi.org/10.48550/arXiv.1810.08771> (2018).
- [30] C. Fu, M. Wang, Q. Hu, L. Zhao, Text-guided co-modulated generative adversarial network for image inpainting, in: 2024 9th International Conference on Big Data Analytics (ICBDA), IEEE, 2024, pp. 92–97, doi:<https://doi.org/10.48550/arXiv.2103.10428>.
- [31] A. Sargsyan, S. Navasardyan, X. Xu, H. Shi, Mi-gan: A simple baseline for image inpainting on mobile devices, in: Proceedings of the IEEE/CVF International Conference on Computer Vision, 2023, pp. 7335–7345, doi:<https://doi.org/10.1109/ICCV51070.2023.00674>.
- [32] H. Liu, Z. Wan, W. Huang, Y. Song, X. Han, J. Liao, Pd-gan: Probabilistic diverse gan for image inpainting, in: Proceedings of the IEEE/CVF

conference on computer vision and pattern recognition, 2021, pp. 9371–9381, doi:<https://doi.org/10.1109/CVPR46437.2021.00925>.

- [33] X. Zhang, X. Wang, C. Shi, Z. Yan, X. Li, B. Kong, S. Lyu, B. Zhu, J. Lv, Y. Yin, et al., De-gan: Domain embedded gan for high quality face image inpainting, *Pattern Recognition* 124 (2022) 108415, doi:<https://doi.org/10.1016/j.patcog.2021.108415>.
- [34] Y. Yu, L. Zhang, H. Fan, T. Luo, High-fidelity image inpainting with gan inversion, in: European Conference on Computer Vision, Springer, 2022, pp. 242–258, doi:<https://doi.org/10.48550/arXiv.2208.11850>.
- [35] Y. Zhou, C. Barnes, E. Shechtman, S. Amirghodsi, Transfill: Reference-guided image inpainting by merging multiple color and spatial transformations, in: Proceedings of the IEEE/CVF conference on computer vision and pattern recognition, 2021, pp. 2266–2276, doi:<https://doi.org/10.48550/arXiv.2103.15982>.
- [36] W. Li, Z. Lin, K. Zhou, L. Qi, Y. Wang, J. Jia, Mat: Mask-aware transformer for large hole image inpainting, in: Proceedings of the IEEE/CVF conference on computer vision and pattern recognition, 2022, pp. 10758–10768, doi:<https://doi.org/10.48550/arXiv.2203.15270>.
- [37] Y. Deng, S. Hui, S. Zhou, D. Meng, J. Wang, T-former: An efficient transformer for image inpainting, in: Proceedings of the 30th ACM international conference on multimedia, 2022, pp. 6559–6568, doi:<https://doi.org/10.1145/3503161.3548446>.
- [38] Q. Dong, C. Cao, Y. Fu, Incremental transformer structure enhanced image inpainting with masking positional encoding, in: Proceedings of the IEEE/CVF conference on computer vision and pattern recognition, 2022, pp. 11358–11368, doi:<https://doi.org/10.48550/arXiv.2203.00867>.
- [39] P. Shamsolmoali, M. Zareapoor, E. Granger, Transinpaint: Transformer-based image inpainting with context adaptation, in: Proceedings of the IEEE/CVF international conference on computer vision, 2023, pp. 849–858, doi:<https://doi.org/10.1109/ICCVW60793.2023.00092>.
- [40] K. Ko, C.-S. Kim, Continuously masked transformer for image inpainting, in: Proceedings of the IEEE/CVF interna-

tional conference on computer vision, 2023, pp. 13169–13178, doi:<https://doi.org/10.1109/ICCV51070.2023.01211>.

- [41] A. Lugmayr, M. Danelljan, A. Romero, F. Yu, R. Timofte, L. Van Gool, Repaint: Inpainting using denoising diffusion probabilistic models, in: Proceedings of the IEEE/CVF conference on computer vision and pattern recognition, 2022, pp. 11461–11471, doi:<https://doi.org/10.48550/arXiv.2201.09865>.
- [42] C. Saharia, W. Chan, H. Chang, C. Lee, J. Ho, T. Salimans, D. Fleet, M. Norouzi, Palette: Image-to-image diffusion models, in: ACM SIGGRAPH 2022 conference proceedings, 2022, pp. 1–10, doi:<https://doi.org/10.48550/arXiv.2111.05826>.
- [43] C. Wei, K. Mangalam, P.-Y. Huang, Y. Li, H. Fan, H. Xu, H. Wang, C. Xie, A. Yuille, C. Feichtenhofer, Diffusion models as masked autoencoders, in: Proceedings of the IEEE/CVF International Conference on Computer Vision, 2023, pp. 16284–16294, doi:<https://doi.org/10.48550/arXiv.2304.03283>.
- [44] R. M. Cichy, A. Khosla, D. Pantazis, A. Torralba, A. Oliva, Comparison of deep neural networks to spatio-temporal cortical dynamics of human visual object recognition reveals hierarchical correspondence, *Scientific reports* 6 (1) (2016) 27755, doi:<https://doi.org/10.1038/srep27755>.
- [45] P. Kok, G. J. Brouwer, M. A. van Gerven, F. P. de Lange, Prior expectations bias sensory representations in visual cortex, *Journal of Neuroscience* 33 (41) (2013) 16275–16284, doi:<https://doi.org/10.1523/jneurosci.0742-13.2013>.
- [46] D. H. Hubel, T. N. Wiesel, Receptive fields, binocular interaction and functional architecture in the cat's visual cortex, *The Journal of physiology* 160 (1) (1962) 106, doi:<https://doi.org/10.1113/jphysiol.1962.sp006837>.
- [47] D. J. Felleman, D. C. Van Essen, Distributed hierarchical processing in the primate cerebral cortex., *Cerebral cortex* (New York, NY: 1991) 1 (1) (1991) 1–47, doi:<https://doi.org/10.1093/cercor/1.1.1-a>.
- [48] O. Ronneberger, P. Fischer, T. Brox, U-net: Convolutional networks for biomedical image segmentation, in: International Conference on Medical

image computing and computer-assisted intervention, Springer, 2015, pp. 234–241, doi:[https://doi.org/10.1007/978-3-319-24574-4\\_28](https://doi.org/10.1007/978-3-319-24574-4_28).

[49] Z. Zhou, M. M. Rahman Siddiquee, N. Tajbakhsh, J. Liang, Unet++: A nested u-net architecture for medical image segmentation, in: International workshop on deep learning in medical image analysis, Springer, 2018, pp. 3–11, doi:<https://doi.org/10.48550/arXiv.1807.10165>.

[50] K. Friston, The free-energy principle: a unified brain theory?, *Nature reviews neuroscience* 11 (2) (2010) 127–138, doi:<https://doi.org/10.1038/nrn2787>.

[51] T. S. Lee, D. Mumford, Hierarchical bayesian inference in the visual cortex, *Journal of the Optical Society of America A* 20 (7) (2003) 1434–1448, doi:<http://dx.doi.org/10.1364/JOSAA.20.001434>.

[52] M. Mirza, S. Osindero, Conditional generative adversarial nets, arXiv preprint arXiv:1411.1784doi:<https://doi.org/10.48550/arXiv.1411.1784> (2014).

[53] L. Itti, C. Koch, Computational modelling of visual attention, *Nature reviews neuroscience* 2 (3) (2001) 194–203, doi:<https://doi.org/10.1038/35058500>.

[54] E. K. Miller, J. D. Cohen, An integrative theory of prefrontal cortex function, *Annual review of neuroscience* 24 (1) (2001) 167–202, doi:<https://doi.org/10.1146/annurev.neuro.24.1.167>.

[55] C. Wang, S. Dong, X. Zhao, G. Papanastasiou, H. Zhang, G. Yang, Saliencygan: Deep learning semisupervised salient object detection in the fog of iot, *IEEE Transactions on Industrial Informatics* 16 (4) (2019) 2667–2676, doi:<https://doi.org/10.1109/TII.2019.2945362>.

[56] K. Nazeri, E. Ng, T. Joseph, F. Z. Qureshi, M. Ebrahimi, Edgeconnect: Generative image inpainting with adversarial edge learning, arXiv preprint arXiv:1901.00212doi:<https://doi.org/10.48550/arXiv.1901.00212> (2019).

[57] G. Kanizsa, Subjective contours, *Scientific American* 234 (4) (1976) 48–53, doi:[https://doi.org/10.1007/978-981-99-6000-2\\_1264-1](https://doi.org/10.1007/978-981-99-6000-2_1264-1).

[58] G. Kanizsa, Seeing and thinking, *Acta psychologica* 59 (1) (1985) 23–33, doi:[https://doi.org/10.1016/0001-6918\(85\)90040-X](https://doi.org/10.1016/0001-6918(85)90040-X).

[59] G. Davis, J. Driver, Parallel detection of kanizsa subjective figures in the human visual system, *Nature* 371 (6500) (1994) 791–793, doi:<http://dx.doi.org/10.1038/371791a0>.

[60] I. Goodfellow, J. Pouget-Abadie, M. Mirza, B. Xu, D. Warde-Farley, S. Ozair, A. Courville, Y. Bengio, Generative adversarial networks, *Communications of the ACM* 63 (11) (2020) 139–144, doi:<https://doi.org/10.48550/arXiv.1406.2661>.

[61] J. Li, S. Chen, S. Wang, M. Lei, X. Dai, C. Liang, K. Xu, S. Lin, Y. Li, Y. Fan, et al., An optical biomimetic eyes with interested object imaging, *arXiv preprint arXiv:2108.04236* doi:<https://doi.org/10.48550/arXiv.2108.04236> (2021).

[62] X. Liao, J. Li, L. Li, C. Shangguan, S. Huang, Rgbd salient object detection, based on specific object imaging, *Sensors* 22 (22) (2022) 8973, doi:<https://doi.org/10.3390/s22228973>.

[63] S. Chen, J. Li, Object of interest extraction based on deep learning, in: Second International Conference on Optics and Image Processing (ICOIP 2022), Vol. 12328, SPIE, 2022, pp. 304–308, doi:<https://doi.org/10.1117/12.2644286>.

[64] J. Li, B. Jia, X. Dai, G. Ou, Q. Luo, Tile quality detection system based on an object imaging method, *Optik* 140 (2017) 1091–1098, doi:<https://doi.org/10.1016/j.ijleo.2017.05.041>.

[65] Y. Wu, M. Liu, J. Li, Detection and recognition of visual geons based on specific object-of-interest imaging technology, *Sensors* 25 (10) (2025) 3022, doi:<https://doi.org/10.3390/s25103022>.

[66] R. Desimone, J. Duncan, et al., Neural mechanisms of selective visual attention, *Annual review of neuroscience* 18 (1) (1995) 193–222, doi:<http://dx.doi.org/10.1146/annurev.ne.18.030195.001205>.

[67] K. M. O’Craven, P. E. Downing, N. Kanwisher, fmri evidence for objects as the units of attentional selection, *Nature* 401 (6753) (1999) 584–587, doi:<https://doi.org/10.1038/44134>.

[68] V. Perry, R. Oehler, A. Cowey, Retinal ganglion cells that project to the dorsal lateral geniculate nucleus in the macaque monkey, *Neuroscience* 12 (4) (1984) 1101–1123, doi:[https://doi.org/10.1016/0306-4522\(84\)90006-x](https://doi.org/10.1016/0306-4522(84)90006-x).

[69] C. Heywood, A. Cowey, On the role of cortical area v4 in the discrimination of hue and pattern in macaque monkeys, *Journal of Neuroscience* 7 (9) (1987) 2601–2617, doi:<http://dx.doi.org/10.1523/JNEUROSCI.07-09-02601.1987>.

[70] J. T. Serences, Voluntary and stimulus-driven attentional control in human cortex, *The Johns Hopkins University*, 2006, doi:<https://doi.org/10.1111/j.0956-7976.2005.00791.x>.

[71] M. Jigo, M. Carrasco, Attention alters spatial resolution by modulating second-order processing, *Journal of Vision* 18 (7) (2018) 2–2, doi:.

[72] A. Barbot, M. Carrasco, Attention modifies spatial resolution according to task demands, *Psychological science* 28 (3) (2017) 285–296, doi:<https://doi.org/10.1167/18.7.2>.

[73] M. Ekman, P. R. Roelfsema, F. P. de Lange, Object selection by automatic spreading of top-down attentional signals in v1, *Journal of Neuroscience* 40 (48) (2020) 9250–9259, doi:<https://doi.org/10.1523/JNEUROSCI.0438-20.2020>.

[74] M. Ekman, S. Kusch, F. P. de Lange, Successor-like representation guides the prediction of future events in human visual cortex and hippocampus, *elife* 12 (2023) e78904, doi:<https://doi.org/10.7554/elife.78904>.

[75] T. Schlegl, P. Seeböck, S. M. Waldstein, G. Langs, U. Schmidt-Erfurth, f-anogan: Fast unsupervised anomaly detection with generative adversarial networks, *Medical image analysis* 54 (2019) 30–44, doi:<https://doi.org/10.1016/j.media.2019.01.010>.

[76] J. Johnson, A. Alahi, L. Fei-Fei, Perceptual losses for real-time style transfer and super-resolution, in: *European conference on computer vision*, Springer, 2016, pp. 694–711, doi:[https://doi.org/10.1007/978-3-319-46475-6\\_43](https://doi.org/10.1007/978-3-319-46475-6_43).

[77] L. A. Gatys, A. S. Ecker, M. Bethge, Image style transfer using convolutional neural networks, in: Proceedings of the IEEE conference on computer vision and pattern recognition, 2016, pp. 2414–2423, doi:<https://doi.org/10.1109/CVPR.2016.265>.

[78] C. Barnes, E. Shechtman, A. Finkelstein, D. B. Goldman, Patchmatch: A randomized correspondence algorithm for structural image editing, *ACM Trans. Graph.* 28 (3) (2009) 24, doi:<https://doi.org/10.1145/1531326.1531330>.

[79] Y. Zeng, J. Fu, H. Chao, B. Guo, Aggregated contextual transformations for high-resolution image inpainting, *IEEE transactions on visualization and computer graphics* 29 (7) (2022) 3266–3280, doi:<https://doi.org/10.1109/TVCG.2022.3156949>.

[80] X. Li, Q. Guo, D. Lin, P. Li, W. Feng, S. Wang, Misf: Multi-level interactive siamese filtering for high-fidelity image inpainting, in: Proceedings of the IEEE/CVF conference on computer vision and pattern recognition, 2022, pp. 1869–1878, doi:<https://doi.org/10.1109/CVPR52688.2022.00191>.

[81] R. Suvorov, E. Logacheva, A. Mashikhin, A. Remizova, A. Ashukha, A. Silvestrov, N. Kong, H. Goka, K. Park, V. Lempitsky, **Resolution-robust large mask inpainting with fourier convolutions**, in: Proceedings of the IEEE/CVF winter conference on applications of computer vision, 2022, pp. 2149–2159.  
URL <http://dx.doi.org/10.48550/arXiv.2109.07161>

[82] R. Zhang, P. Isola, A. A. Efros, E. Shechtman, O. Wang, The unreasonable effectiveness of deep features as a perceptual metric, in: Proceedings of the IEEE conference on computer vision and pattern recognition, 2018, pp. 586–595, doi:<https://doi.org/10.1109/CVPR.2018.00068>.

[83] P. R. Roelfsema, V. A. Lamme, H. Spekreijse, Object-based attention in the primary visual cortex of the macaque monkey, *Nature* 395 (6700) (1998) 376–381, doi:<https://doi.org/10.1038/26475>.